1

2 **Antagonistic relationship of NuA4 with the Non-Homologous End-Joining**

3 **machinery at DNA damage sites**

4

5

6 Salar Ahmad[1], Valerie Côté[1], Xue Cheng[1], Gaëlle Bourriquen[1], Vasileia Sapountzi[1], Mohammed

7 Altaf[1,#a] and Jacques Côté[1]*

8

9

10 [1] St-Patrick Research Group in Basic Oncology, Centre Hospitalier Universitaire de Québec-

11 Université Laval Research Center, Laval University Cancer Research Center, Quebec City, QC,

12 Canada

13 [#a] Current address: Chromatin and Epigenetics Lab, Department of Biotechnology, University of

14 Kashmir, Srinagar, Jammu and Kashmir 190006, India

15

16 * Corresponding authors: jacques.cote@crhdq.ulaval.ca (JC)

17

18 **Running Title:** Reciprocal antagonistic interplay between NuA4 and NHEJ factors

19

20

Abstract

The NuA4 histone acetyltransferase complex, apart from its known role in gene regulation, has also been directly implicated in the repair of DNA double-strand breaks (DSBs), favoring homologous recombination (HR) in S/G2 during the cell cycle. Here, we investigate the antagonistic relationship of NuA4 with non-homologous end joining (NHEJ) factors. We show that budding yeast Rad9, the 53BP1 ortholog, can inhibit NuA4 acetyltransferase activity when bound to chromatin *in vitro*. While we previously reported that NuA4 is recruited at DSBs during the S/G2 phase, we can also detect its recruitment in G1 when genes for NHEJ factors Rad9, Yku80 and Nej1 are mutated. This is accompanied with the binding of single-strand DNA binding protein RPA and Rad52, indicating DNA end resection in G1 as well as recruitment of the HR machinery. This NuA4 recruitment to DSBs in G1 depends on both Xrs2 and Lcd1/Ddc2 and is linked to the hyper-resection phenotype of NHEJ mutants. It also implicates NuA4 in the resection-based single-strand annealing (SSA) repair pathway along Rad52. Interestingly, we identified two novel non-histone acetylation targets of NuA4, Nej1 and Yku80. Acetyl-mimicking mutant of Nej1 inhibits repair of DNA breaks by NHEJ, decreases its interaction with other core NHEJ factors such as Yku80 and Lif1 and favors end resection. Altogether, these results establish a strong reciprocal antagonistic regulatory function of NuA4 and NHEJ factors in repair pathway choice and suggests a role of NuA4 in alternative repair mechanism that involves DNA-end resection in G1.

Author Summary

DNA double-strand breaks (DSBs) are one of the most harmful form of DNA damage. Cells employ two major repair pathways to resolve DSBs: Homologous Recombination (HR) and Non-

43 Homologous End Joining (NHEJ). Here we wanted to dissect further the role played by the NuA4
44 (Nucleosome acetyltransferase of histone H4) complex in the repair of DSBs. Budding yeast NuA4
45 complex, like its mammalian homolog TIP60 complex, has been shown to favor repair by HR.
46 Here, we show that indeed budding yeast NuA4 and components of the NHEJ repair pathway
47 share an antagonistic relationship. Deletion of NHEJ components enables increased recruitment
48 of NuA4 in the vicinity of DSBs, possible through two independent mechanisms, where NuA4
49 favors the end resection process which implicates it in repair by single-strand annealing (SSA), an
50 alternate homology-based repair pathway. Additionally, we also present two NHEJ core
51 components as new targets of NuA4 acetyltransferase activity and suggest that these acetylation
52 events can disassemble the NHEJ repair complex from DSBs, favoring repair by HR. Our study
53 demonstrates the importance of NuA4 in the modulation of DSB repair pathway choice.
54
55

56 **Introduction**

57 The genomic integrity of a cell is under constant assault from various endogenous and exogenous
58 sources. One of the most deleterious manifestation is DNA double strand breaks (DSBs), as failure
59 to repair a DSB can lead to loss of genetic information and be an underlying cause for tumor
60 progression in higher eukaryotes [1, 2]. Cells have two main pathways to repair DSBs. First,
61 Homologous Recombination (HR) is carried out in the S/G2 phase of the cell cycle, relies on 5'-3'
62 resection of the broken DNA ends and uses the homology on the sister chromatid as a template
63 for repair [3]. Second, Non-Homologous End Joining (NHEJ) is carried out throughout the cell
64 cycle but it is the dominant form of repair in the G1 phase. NHEJ may or may not use processing
65 of the broken ends before ligation, making it a more error-prone pathway than HR [4]. Cells also
66 have backup repair pathways such as Single Strand Annealing (SSA) and alt-NHEJ, which share
67 some components with HR and NHEJ, respectively. These pathways come into play under special
68 conditions when the main repair pathways are hindered due to genetic mutations, absence of
69 sister chromatid and state of the cell cycle [5, 6].

70 The yeast NuA4 histone acetyltransferase complex is essential for cell viability, is
71 composed of 13 subunits and is homologous to the mammalian TIP60/p400 complex [7, 8].
72 NuA4/TIP60 acetylates histones H4 and H2A N-terminal tails in chromatin, as well as variants
73 H2A.X/H2A.Z [9-13]. NuA4/TIP60 has been well documented for its role in transcription
74 regulation, at the initiation and elongation steps [14, 15]. NuA4 is also known to acetylate non-
75 histone proteins and regulate a variety of cellular processes such as autophagy and
76 gluconeogenesis [16, 17]. Temperature sensitive mutants of Esa1, the yeast catalytic subunit, as
77 well as point mutants of H4 and H2A target lysine residues show growth defects in presence of

78 various DNA damaging chemical agents, underpinning the importance of NuA4 and acetylation
79 for the repair of DNA breaks [7, 9, 18-20]. NuA4 has been shown to play an important role for the
80 recruitment of chromatin remodelers such as INO80, SWI/SNF and RSC to DNA repair sites [20-
81 22]. We have shown that NuA4 is rapidly recruited to a DSB by the MRX complex (Mre11-Rad50-
82 Xrs2) and this is most likely through a DNA damage-induced phospho-dependent interaction with
83 the Xrs2 protein [23]. Very recently, we found that NuA4 is recruited to DSBs along another
84 important HAT complex, SAGA, and their combined action is essential for DNA end resection to
85 occur and HR [24]. In addition, we have shown that NuA4 directly acetylates RPA to modulates
86 its dynamic association with ssDNA during the repair process [23]. NuA4 has also been implicated
87 in opposing Rad9 checkpoint activity after DNA damage in budding yeast [10, 25]. This is
88 paralleled by the mammalian TIP60 complex which was shown to antagonize 53BP1 (homolog of
89 yeast Rad9) in the vicinity of DSBs to favor repair by HR [26, 27]. Tip60-dependant acetylation
90 and activation of ATM has also been argued to be involved in DNA damage signaling [28].

91 In this study we dissected the functional relationship of NuA4 with the NHEJ repair
92 pathway. We show that, upon removal of NHEJ factors, NuA4 is strongly recruited to DSBs during
93 the G1 phase of the cell cycle, alongside DNA end resection, in a Xrs2 or Lcd1/Ddc2-dependent
94 manner. Conditions of defective NuA4 acetyltransferase activity decrease the hyper-resection
95 phenotype of NHEJ mutants, implicating NuA4 in the resection-based SSA repair pathway in G1.
96 In addition, NHEJ core factors Nej1 and Yku80 are targets of NuA4-dependent acetylation which
97 lowers NHEJ efficiency, disrupts physical interactions and increases resection. Our results support
98 a model in which NuA4 and the NHEJ machinery are negatively regulating each other, NuA4
99 favoring repair of DSBs by resection-based pathways in part through inhibition of NHEJ factors.

100

101 ## Results

102 **Deletion of NHEJ factors leads to recruitment of NuA4 at DSBs in G1**

103 Yeast Rad9, similar to its mammalian homolog 53BP1, is known to slow down or to keep a check
104 on the rate of DNA end resection [29-32]. 53BP1 has been shown to have an antagonistic
105 relationship with mammalian NuA4/TIP60 [27]. They compete to bind the H4K20me mark and
106 target H2AK15 modifications, implicating them in the selection of the DSB repair pathway [26].
107 In yeast, NuA4 mutant cells accumulate in the G2 phase at non-permissive temperature, in a
108 Rad9-dependent manner [10]. In addition, NuA4 mutants defective in acetylation show a strongly
109 increased Rad9-dependent G1 checkpoint upon DNA damage, implicating NuA4 in an
110 antagonistic relationship with Rad9 during the DNA damage response [25].

111 Yeast Rad9 binds chromatin near DSBs through bivalent interaction with two histone
112 marks, H3K79me by its Tudor domain and H2AS129ph by its BRCT domain (γH2A) [33-35]**.** To
113 determine if Rad9 binding to chromatin can affect NuA4 activity (**Fig 1A**), we performed *in vitro*
114 histone acetyltransferase (HAT) assays using native chromatin purified from cells treated with a
115 DNA damaging agent, MMS. Wild type and Tudor or BRCT mutant recombinant Rad9 (aa639-
116 1308, **S1A Fig**) were incubated with chromatin and purified native NuA4 complex, followed by
117 HAT assay with radioactive Acetyl-CoA. Wild type Rad9 was able to significantly block acetylation
118 of nucleosomes by NuA4, whereas Rad9-Y798Q and Rad9-K1088E were significantly less efficient
119 at doing so, reflecting their decreased ability to bind chromatin (**Fig 1B and S1B Fig**).

120 We and others have shown that NuA4 is recruited to DSBs mainly during the S/G2 phase
121 of the cell cycle [23, 36]. To study whether Rad9 may affect recruitment of NuA4 at DSBs *in vivo*,

122 we deleted *RAD9* and performed chromatin immunoprecipitations (ChIP)-qPCR at the HO-
123 induced DSB in asynchronous and G1-arrested cells. It is important to indicate that all the ChIP
124 experiments presented in this study were controlled for consistent level of HO-induced DSB
125 formation (**S1E-I Fig**) as well as tight synchronization of cells in G1 (*bar1* mutant background,
126 FACS and microscopic analysis). While asynchronous cells showed no significant difference in
127 NuA4 binding between wild type and *RAD9* deletion mutant (**S1C Fig**), G1 synchronized cells
128 showed a small but significant increase in the recruitment of NuA4 (**Fig 1C**), along with the
129 expected increase of DNA end resection as measured with Rfa1, the largest subunit of RPA (**Fig**
130 **1D**).

131 Deletion of yeast Ku (Yku) in asynchronous cells did not significantly affect recruitment of
132 NuA4 at the HO-induced DSB [23]. However, cells synchronized in G1 phase showed strong
133 recruitment of NuA4 at the DSB in the absence of Yku80 (**Fig 1E**), reminiscent of a reported
134 increased binding of some proteins shared by RPD3S, SWR-C and NuA4 complexes in the absence
135 of Yku70 [36]. ChIPs with Rfa1 also showed strongly increased signal for RPA around the DSB site,
136 indicating abnormal high DNA end resection in G1 (**Fig 1F**). We wanted to know if this antagonistic
137 relationship was exclusive for Yku or extended to other NHEJ factors. Deletion of *NEJ1*, a core
138 NHEJ factor, in G1 synchronized cells resulted again in increased NuA4 recruitment around the
139 HO DSB (**Fig 1G),** as well as higher resection (**Fig 1H**), which is not observed in asynchronous cells
140 (**S1D Fig**).

141 In parallel, *RAD9* was deleted in the *YKU80* deleted background. Previous studies have
142 shown that the double deletion of *RAD9* and *YKU70* results in hyper-resection of DNA ends at
143 DSBs in the G1 phase of the cell cycle [37]. We confirmed this finding as indicated by a very strong

144 increase of Rfa1 signal seen in *rad9*Δy*ku80*Δ cells (**Fig 1F**). Interestingly, a similar effect was
145 observed for NuA4, with the double deletion mutant giving a much stronger signal compared to
146 single y*ku80*Δ cells (**Fig 1E**). Altogether, these data demonstrate that the NuA4 complex can be
147 efficiently recruited at a DSB in G1 in the absence of core NHEJ factors, Yku80 and Nej1, and also
148 with the deletion of *RAD9*. This supports the concept of an antagonistic relationship between
149 NuA4 and the NHEJ machinery for repair of DNA breaks.
150

151 **Xrs2-dependent recruitment of NuA4 at DSB in G1**

152 NuA4 subunit Tra1 shows high domain homology with Tel1/ Mec1, members of the PIKK family.
153 Both Tel1 and Mec1, like their mammalian counterpart ataxia telangiectasia mutated (ATM), AT-
154 related (ATR) and DNA-dependent protein kinase (DNA-PK), are important for signaling of the
155 DSB and recruitment of downstream repair proteins [38, 39]. We have recently shown that Tra1
156 gets phosphorylated upon DNA damage and its C-terminus containing the PI3K-like domain can
157 directly bind Xrs2 *in vitro*, an interaction likely involved in the recruitment of NuA4 at the HO
158 induced DSB site [23]. To understand if Xrs2 is required for NuA4 recruitment at the DSB in G1,
159 we performed ChIP-qPCR in *XRS2* deletion background. As seen in (**Fig 2A**), the NuA4 signal
160 detected in G1 in the absence of Rad9 was completely lost when *XRS2* is deleted. The same can
161 be said for end resection measured by Rfa1/RPA (**Fig 2B**). Strikingly, deletion of *XRS2* in the
162 background with hyper-resection (*rad9*Δy*ku80*Δ) also abrogated NuA4 recruitment and resection
163 in G1 cells (**Fig 2C-D and S2D Fig**). We have previously shown that NuA4 is recruited through a
164 two-step mechanism at DSBs in S/G2: first, by the MRX complex, through the phospho-
165 dependent interaction with Xrs2; and second, by spreading on each side of the break along DNA

166 end resection [23]. Since deletion of *XRS2* blocks resection, it was unclear whether the loss of
167 NuA4 recruitment is solely due to the loss of interaction with Xrs2 or also partly due to the loss
168 of resection itself. The *mre11-H125N* nuclease-defective mutant background was used to partly
169 address this issue since it is known to slow down the rate of resection in G1 synchronized cells
170 [40]. As shown in **Fig 2E-F**, while there was a decrease in the Rfa1 signal close to the break, NuA4
171 detection seemed unaffected. These results suggest that NuA4 recruitment at a DSB in G1
172 requires the Xrs2 subunit of the Mre11/Rad50/Xrs2 (MRX) complex, in a resection-independent
173 manner.
174
175 **Lcd1/Ddc2-dependent recruitment of NuA4 at DSBs**
176 Xrs2 harbors the Nuclear Localization Sequence (NLS) required for Mre11 import into the
177 nucleus. Thus, loss of Xrs2 results in failed assembly of the MRX complex at the DSB [41]. To
178 overcome this issue, we used a low copy number plasmid expressing Mre11 fused to a NLS
179 (referred to as *MRE11-NLS*). In accordance with previous studies, expression of Mre11-NLS
180 suppressed the growth defect of *xrs2*Δ cells in the presence of a DNA damaging agent (MMS, **S3A**
181 **Fig**) [41, 42]. Interestingly, expression of Mre11-NLS in G1 cells carrying the double deletion
182 *rad9*Δy*ku80*Δ in addition to *xrs2*Δ led to a significant increase in NuA4 recruitment and resection
183 (**Fig 3A-B**). Since the suppression of *xrs2Δ* by Mre11-NLS is known to be partial, we also tested
184 the Mre11-NLS-X85 fusion which adds the C-terminal 85aa Tel1-interacting domain of Xrs2 to
185 Mre11 [43] (distinct from the N-terminal FHA-BRCT NuA4-interacting domain [23]). This
186 construct led to an even much stronger increase of NuA4 recruitment and resection at the DSB
187 in the absence of Xrs2, Rad9 and Yku80 (**Fig 3C-D**). These results demonstrate the existence of an

188 Xrs2-independent mode of NuA4 recruitment at DSBs. Importantly, this Xrs2-independent
189 mechanism is not restricted to cells in G1 as asynchronous cells also show a rescue for NuA4
190 recruitment and resection with the introduction of *MRE11-NLS* in *xrs2*Δ cells (**Fig 3E-F**).

191 We previously reported that the Tra1 subunit of NuA4 can interact directly *in vitro* with
192 Lcd1/Ddc2 (ATRIP in mammals) [23]. Lcd1/Ddc2 is the binding partner of Mec1 (ATR in mammals)
193 and is responsible for the recruitment of Mec1 onto the RPA-coated ssDNA generated by
194 resection [44]. Importantly, we have previously shown that deletion of *LCD1/DDC2* did not
195 significantly affect the recruitment of NuA4 at the HO break in asynchronous cells [23](see also
196 **S4B Fig**). To establish whether NuA4 interaction with Lcd1/Ddc2 could be in fact an alternate
197 mechanism of NuA4 recruitment when Xrs2 function is genetically bypassed (as above), we
198 deleted *LCD1* (in a *SML1* deleted background to overcome the synthetic lethality) [45, 46].
199 However, the introduction of *MRE11-NLS* in this background is insufficient to rescue resection,
200 making conclusions about NuA4 recruitment difficult (**S4A-B Fig**). To overcome this issue, we
201 overexpressed long range resection exonuclease Exo1. Expression of Mre11-NLS along with Exo1
202 overexpression led to diminished DNA signals on each side of the break after HO induction,
203 indicating DNA end resection (**Fig 4A,C**)**.** This is dependent on Exo1 activity since a nuclease dead
204 mutant of the protein (Exo1-D173A) behaves like the empty vector control (EV). In conditions of
205 *XRS2* deletion partly suppressed by Mre11-NLS, the expression of active Exo1 led to a further
206 increase of NuA4 recruitment (**Fig 4B**). However, when *LCD1/DDC2* was deleted in these
207 conditions that allow significant DNA end resection (**Fig 4C**), NuA4 signals failed to increase (**Fig**
208 **4D**). Therefore, these results indicate that, in conditions in which Xrs2 function is genetically

209 bypassed, there is an alternate Lcd1/Ddc2-dependent mechanism of NuA4 recruitment at the
210 DNA break, likely through a direct physical interaction.
211
212 **NuA4-dependent acetylation is important for hyper-resection in G1 cells and repair by the SSA**
213 **pathway**
214 DSBs flanked by direct repeats are repaired by a Rad52-dependent pathway called single strand
215 annealing (SSA). The resected ends anneal at the repeats and the intervening DNA along with one
216 repeat are removed by a nucleolytic process [47]. It has been well documented that Rad52 is
217 essential for repair of DSBs by SSA in G1 cells [37]. To investigate NuA4 possible function in such
218 process, we performed ChIP-qPCR to measure Rad52 recruitment to DSBs in G1 and our mutant
219 backgrounds. As expected in the hyper-resection *rad9*Δy*ku80*Δ mutant background, very high
220 recruitment of Rad52 was detected in G1 cells (**Fig 5A**). This was also seen in the *nej1*Δ
221 background, albeit to a lower level similar to the y*ku80*Δ single mutant (**Fig 5A-B**). Similar to a
222 previous study [48], we also observed recruitment of Rad51 in y*ku80*Δ and *rad9*Δy*ku80*Δ G1-
223 blocked cells (**S5A Fig**).
224 To determine whether NuA4 has a role in this G1 phase mechanism of DSB repair, we
225 introduced the *esa1-L254P* temperature sensitive (ts) mutant allele which affects the acetylation
226 capacity of NuA4 even at semi-restrictive temperature (as shown by western blot for the H4ac in
227 **Fig 5C)**[10]. Interestingly, Rfa1 ChIP-qPCR to measure the hyper-resection phenotype in the triple
228 *rad9*Δy*ku80*Δ*esa1-ts* triple mutant background showed a significant reduction of DNA end
229 resection compared to the *rad9*Δy*ku80*Δ double mutant (**Fig 5D**). These results indicate that
230 NuA4 acetyltransferase activity is important to stimulate DNA end resection in G1, likely in part

231 through acetylation of chromatin in front of the resection machinery. This was supported by a
232 partial suppression of the DNA damage sensitivity of *esa1-ts* mutant cells by the *rad9*Δy*ku80*Δ
233 deletions (**Fig 5E**). On the other hand, we did not observe a clear effect of NuA4 partial loss of
234 function on Rad52 recruitment in these conditions in G1 cells (**S5B Fig**).

235 To directly assess the possible role of NuA4 in the repair of DSBs by the SSA pathway, we
236 used a yeast reporter strain carrying two regions of homology (direct repeats) separated by 20
237 kb [49]. When the Rad51 recombinase is removed from this background, repair of the HO break
238 occurs by the SSA pathway that requires Rad52. Growth (spot assays) in conditions of HO
239 induction is used as measure of DNA repair. Deletion of *RAD52* in this background created a
240 strong growth defect after HO induction, as expected since SSA is abrogated (**Fig 5F**). Importantly,
241 the *esa1 ts* allele in combination with *RAD51* deletion led to a similar growth defect upon HO
242 induction, suggesting that NuA4 is important for repair of DNA breaks by the resection-
243 dependent SSA pathway (**Fig 5F**).

244

245 **Acetylation of Nej1 by NuA4 as a mechanism to inhibit NHEJ, favoring resection-based repair**

246 Yeast Nej1 and its mammalian homologs XLF/NHEJ1 and PAXX have been shown to be important
247 for repair by NHEJ [50-53]. Nej1 acts as a scaffolding protein for other NHEJ factors, the N-
248 terminal region of Nej1 interacting with Yku and its C-terminal region with Lif1 [54-56]. XLF has
249 also been shown to interact with mammalian Ku and XRCC4 [54]. Both Nej1 and Dnl4-Lif1 are
250 required for retention/stabilization of Yku at DSBs [48, 57]. Nej1, like its mammalian homolog, is
251 important for tethering the two broken ends of the DNA [58, 59] and it was also recently shown
252 to interact with Mre11 of the MRX complex for its tethering activity [60].

253 In a large-scale *in vitro* acetylation assay on microarrays, Nej1 was shown to be a target
254 of NuA4 acetyltransferase activity [17]. To investigate this further, we directly tested a
255 recombinant Nej1 protein in acetyltransferase assays *in vitro* with purified NuA4 complex.
256 Migration of the radioactive assay on gel and fluorography clearly indicated efficient acetylation
257 of Nej1 by NuA4 (**Fig 6A**). To determine if Nej1 is indeed acetylated on lysine residues in vivo, we
258 performed immunoprecipitations with an anti-acetyl-lysine antibody on extracts from cells
259 expressing or not a Nej1 fusion protein in normal growth conditions or after MMS-induced DNA
260 damage. The results showed that a small proportion of Nej1 seems indeed acetylated *in vivo*
261 while DNA damage has no impact on the level modification (**Fig 6B**). We then purified this Nej1
262 fusion protein from yeast cells and compared the acetylated lysine-containing peptides identified
263 by mass spectrometry from wild type and the *esa1-L254P* NuA4 mutant backgrounds (**S2 Table**).
264 Three lysine residues, at positions K18, K192 and K234, were detected as being acetylated on
265 Nej1 in WT conditions but not in the mutant background (**Fig 6C**, **S6A Fig**). To determine if these
266 acetylation sites are important for Nej1 function, we produced yeast strains that express
267 physiological levels of Nej1 with non-acetylatable (K to R) or acetylation-mimic (K to Q)
268 substitutions. Importantly, the point mutations did not affect the stability of Nej1 (**Fig 6D**). Next,
269 we tested if these lysines affect the efficiency of DSB repair by NHEJ. As shown in **Fig 6E**, loss of
270 Nej1 completely abrogated repair by NHEJ, measured by re-ligation efficiency of digested plasmid
271 templates. Interestingly, both acetyl (3KQ) as well as non-acetyl (3KR) substitution mutants
272 showed significantly decreased NHEJ efficiency. These results demonstrate the importance of
273 these three lysine residues in Nej1 function during DSB repair by NHEJ. In contrast, Nej1 wild type
274 and mutants show similar repair efficiency for a chromosomal DSB at the *MAT* locus (**S6B Fig**).

275 Importantly, ChIP-qPCRs for NuA4 and RPA around the HO-induced DSB in G1 cells showed
276 significantly increased recruitment of NuA4 as well as resection in the acetyl mimicking *nej1*
277 mutant (**Fig 6F-G**; the non-acetyl *nej1* mutant datapoints overlap with the wild type ones). On
278 the other hand, the increases seen in the *nej1-3KQ* background did not reach the levels obtained
279 with the complete loss of Nej1. This could be due to Nej1-3KQ still getting recruited at the break,
280 but with impaired function. Since Nej1 interaction with other NHEJ factors is important for its
281 function [55-57, 60, 61], we performed *in vitro* protein-protein interaction analysis using Nej1
282 mutants with recombinants Yku80 and Lif1. While wild-type Nej1 and the 3KR mutant showed
283 similar interaction with Yku80, the acetyl mimicking 3KQ mutant showed less binding (**Fig 6H**). In
284 parallel, interaction of Nej1 with Lif1 was significantly decreased in both 3KQ and 3KR mutants
285 compared to wild type (**Fig 6I**). The decreased binding of Nej1-3KR with Lif1 but not with Yku80
286 could explain its effect on the plasmid re-ligation assay (**Fig 6E**). Lif1 binds the Dnl4 ligase and loss
287 of a stable interaction with Nej1 may result in defective Lif1-Dnl4 recruitment, leading to
288 impaired DSB religation. However, since Nej1-3KR is still able to interact with Yku80, stabilizing it
289 at the break, it can explain the absence of effect on resection compared to wild type cells (**Fig**
290 **6G**). Furthermore, the Nej1-3KQ acetyl-mimic mutant also showed decreased binding to the C-
291 terminal part of Mre11 compared to wild type and the 3KR mutant, which may affect its tethering
292 activity (**S6D Fig**). Importantly, Nej1 phosphorylation in response to DNA damaging agents [62]
293 was not affected by the 3 lysine substitutions or the depletion of NuA4 acetyltransferase activity
294 (Esa1) using the anchor-away system [63, 64](cells were treated with DNA damaging agent MMS,
295 phosphorylation leading to the appearance of a slower migrating Nej1 signal) (**S6E-G Fig**).

296 In mammals, NHEJ core factor Ku70 is known to get acetylated by CBP which inhibits DNA
297 repair and regulates Bax-mediated cell apoptosis [65, 66]. We tested if yeast Ku is also acetylated
298 in yeast cells and if it could be a non-histone target of NuA4, along with Nej1. Using the anchor-
299 away system to deplete Esa1 (**S6G Fig**) and immunoprecipitation with an anti-acetyl-lysine
300 antibody, we found that Yku80 was indeed acetylated *in vivo* and NuA4 was clearly required for
301 most of this acetylation to occur (**Fig 6J**). Interestingly, Yku80 acetylation seemed slightly higher
302 in conditions of DNA damage. Taken together, these data indicate that Nej1 and Yku80 are non-
303 histone substrates of NuA4 acetyltransferase activity. Acetylation of Nej1 may reduce NHEJ
304 efficiency by disrupting its interaction with Yku80 and Lif1. Further studies are required to
305 characterize the effect of acetylation on Yku80 function but work in higher eukaryotes also
306 supports an inhibitory role.
307

308 **Discussion**

309 Altogether, the results of this study allowed us to clearly demonstrate a reciprocal antagonistic
310 relationship between the NuA4 complex and the NHEJ machinery, confirming earlier genetic
311 interaction data and our work with mammalian homologs. The *in vitro* and *in vivo* data also went
312 much farther by showing a clear inhibition of NuA4 recruitment and activity on chromatin by
313 NHEJ factors. Strikingly, In the other direction, our data showed that NuA4 can directly inhibits
314 the NHEJ machinery by acetylating some of them. Through this work, we also uncovered a new
315 alternate mode of recruitment for NuA4 at DSBs in specific conditions. The Xrs2-dependent
316 pathway is responsible for initial recruitment of NuA4 in G1 (**Fig 2**), as we previously reported in
317 S/G2 [23]. This happens early during DSB signaling and the repair process when MRX is recruited

318 to the break site. It is known that PIKK family member Tra1, subunit of NuA4, can directly interact
319 with Xrs2 [23]. The other main acetyltransferase complex in yeast, SAGA, also contains Tra1 and
320 requires Xrs2 for its recruitment at the break [24]. Tra1 is therefore related to the Tel1(ATM)
321 signaling kinase not only at the amino acid sequence but also in its mode of recruitment at the
322 DNA break being dependent on Xrs2 [42]. Tel1 signals the DSB by phosphorylation of H2A-S129
323 (γ-H2A) in the surrounding chromatin [67]. The nucleolytic processing, termed resection of the
324 DNA breaks produces 3' ssDNA ends. This ssDNA gets coated by RPA to prevent secondary
325 structure formation and degradation. RPA-coated ssDNA is recognized by various repair proteins,
326 one such being Lcd1/Ddc2(ATRIP) [3, 44]. We had shown previously that Tra1 can also directly
327 interact with Lcd1 *in vitro* [23]. Our *in vivo* data now support this link as NuA4 can still be recruited
328 at the break in specific conditions where Xrs2 function is genetically bypassed and resection can
329 occur, and this recruitment requires Lcd1/Ddc2 (**Fig 3 and 4**). Since the simple deletion of
330 *LCD1/DDC2* in normal conditions had no effect on NuA4 recruitment at DSBs [23](**S4B Fig**), this
331 indicates that Lcd1/Ddc2 is an alternate mode of recruitment occurring only in specific
332 conditions. Nevertheless, it is tempting to speculate a function of this mechanism in the
333 spreading of NuA4 along resection on each side of the break after initial recruitment by MRX (the
334 two-step recruitment model described in [23]). This alternate mode may also be more important
335 specifically during G1 in hyper-resection conditions when the NHEJ machinery is defective.

336 Resection is the event that marks the commitment of DSB repair to the HR process. The
337 3' ended ssDNA searches for the homologous sequence or sister chromatid to use as a template
338 to complete the repair process [3]. Resection is a very regulated process and is active in S/G2
339 phase when the Cdk1 activity is high and inhibited during the G1 phase of the cell cycle when

340 Cdk1 activity is low [37]. But it has been shown previously that resection can be achieved in G1
341 phase with the deletion of Ku protein [37, 48]. In mammalian cells, HR in G1 phase requires
342 deletion of the *RAD9* homolog 53BP1, depletion of KEAP1 and a phospho-mimicking mutant of
343 CtIP [68]. In our experiments we detect efficient NuA4 recruitment at a DSB in G1 concomitant
344 with the appearance of resection (**Fig 1**). It was previously shown that deletion of NHEJ factors in
345 G1 not only leads to resection but also repair of the DSB by SSA, relying on the recombination
346 protein Rad52 [37]. Our question then was to evaluate if NuA4 played a role in this resection-
347 based repair in G1. Temperature sensitive mutant of Esa1, the catalytic subunit of NuA4, slows
348 down resection which likely impairs such repair process requiring extended end resection (**Fig**
349 **5D**). Indeed, using a SSA reporter strain, the *esa1* defective allele creates a clear growth defect
350 when the HO break is induced in that background (**Fig 5F**). Importantly, this implicates the NuA4
351 complex in another DSB repair pathway beside HR. It will be interesting to verify if the SAGA HAT
352 complex also collaborates with NuA4 in this pathway, like it does in HR [24].

353 The antagonistic relationship between NuA4 and the NHEJ machinery seems central to
354 the mechanisms regulating the repair pathway choice. The fact that two NHEJ core factors, Nej1
355 and Yku80, are new non-histone targets of NuA4 acetyltransferase activity (**Fig 6**) is likely an
356 important part of these regulatory events. Nej1 is critical for repair by NHEJ [50, 51, 53] and our
357 *nej1* acetyl mutants also show impaired NHEJ (**Fig 6E**). Nej1 is known to act as a scaffold for
358 binding and stabilizing other proteins of the NHEJ machinery [54-57]. Nej1 acetyl-mimicking
359 mutant shows reduced binding to Lif1 and Yku80 *in vitro*, which correlates with increased
360 resection seen *in vivo* (**Fig 6G**). It will be interesting to determine how these individual lysines
361 affect interaction of Nej1 with other NHEJ proteins and whether the tethering activity of Nej1

362 itself is impaired in these mutants [60]. In both yeast and mammals, it has been documented that
363 Ku may interact with various histone deacetylases (HDACs) and these have an important role in
364 repair by NHEJ [69-71]. Further analysis of NuA4 interplay with NHEJ would include identification
365 of the specific lysines on Yku80 that get acetylated by NuA4. Removal of positive charge of lysines
366 through acetylation may reduce or abrogate the binding capacity of Yku80 to DNA at the break
367 site leading to processing/ resection of the DNA ends. The acetylation may also affect the binding
368 with Yku70 and formation of the Ku complex, thereby impairing NHEJ.

369 **Fig 6** presents a model, based on our data, for the antagonistic relationship between
370 NuA4 and the NHEJ machinery at DNA breaks. NuA4 can be recruited by the MRX complex in the
371 early steps after DSB formation. Since Rad9 and other NHEJ factors get assembled at the break,
372 these, apart from inhibiting resection, may also inhibit recruitment of NuA4 and acetylation of
373 chromatin. If NuA4 is able to directly acetylate Nej1, this blocks the assembly of the NHEJ repair
374 machinery, thereby favoring the initiation of DNA end resection. Resection then leads to RPA-
375 coated ssDNA, recruitment of Lcd1/Ddc2(ATRIP) and NuA4 spreading on each side away from the
376 break, helping long-range resection in the context of chromatin. In the situation of Xrs2 absence
377 or bypass, NuA4 can also be recruited by Lcd1/Ddc2. Our results clearly demonstrate that NuA4
378 regulates the repair pathway choice, away from NHEJ, and favors repair by resection-based
379 processes throughout the cell cycle. It supports and greatly broadens the conclusions of our
380 previous work that highlighted a crucial battle between 53BP1 (mammalian Rad9) and
381 NuA4/TIP60 to regulate DSB repair pathway choice. Future work will verify if the mammalian
382 NuA4/TIP60 complex also targets NHEJ proteins during regulation of repair pathway choice.
383 Interestingly, it has been recently shown that 53BP1 can also be acetylated *in vivo*, which inhibits

384 repair by NHEJ and favors HR [72]. It is also possible that NuA4 is involved in other DSB repair
385 pathways such as alt-NHEJ, underpinning its role in resection-based repair. A better
386 understanding of how NuA4/TIP60 gets recruited to the DNA damage site and acetylates specific
387 non-histone proteins to modulate repair, identifies new molecular targets that can be acted upon
388 to treat diseases such as cancer.
389
390

391 **Methods**

392 **Yeast strains and growth assay**

393 Yeast strains used in the current study are listed in S1 Table. Standard PCR based protocol was
394 used for respective transformations employing the lithium acetate method. Yeast cells were
395 grown in YPD (1% yeast extract, 2% peptone, 2% dextrose) at 30°C or in synthetic complete
396 media. For DSB induction, cells were grown at 30 ^{o}C overnight in YP-Raffinose and 2% galactose
397 was added for 3 hours to induce HO endonuclease.

398 Yeast spot assays were performed with yeast culture grown overnight in YPD at 23°C and
399 SC-URA at 30°C, inoculated in the morning in YPD/ SC-URA at OD_{600} 0.3 and grown for 3–4 hours.
400 The 10-fold serial dilutions of the yeast cultures were made for spotting on YPD/ SC-URA plates
401 supplemented with methylmethane sulfonate (MMS). Colonies were allowed to grow for 3-4
402 days at 32°C for YPD and 30°C for SC-URA plates and the growth sensitivities were compared to
403 YPD/ SC-URA control plate.

404 **Chromatin Immunoprecipitation (ChIP)**

405 ChIP-qPCR was performed as described previously [15]. In short, yeast cells were grown in YP-
406 Raff till optical density (O.D. 600) of the culture was between ~0.5 to 1. α-factor was added to
407 the indicated experiments for 6 hours to synchronize the cells in G1 phase. This was followed by
408 addition to galactose for 3 hours to induce DSB at MAT locus. Next, cells were cross-linked with
409 formaldehyde and cells were lysed by bead beating. Sonication was performed (Diagenode
410 Bioruptor) to obtain chromatin size of ~200-500 bp. 100ug of chromatin was incubated with the
411 indicated antibody overnight on a wheel at 4°C. Next day, protein A or G sepharose beads were
412 added followed by subsequent washing steps and overnight at 65°C for de-crosslinking. Phenol

413 chloroform extraction was performed, and DNA samples were dissolved in NTE to be used for
414 qPCR. LC480 LightCycler (Roche) was used to quantify DNA with the primer pairs flanking the
415 indicated region left (0.15bp, 1Kb, 3Kb, 7Kb) and right (1kb, 3Kb, 7Kb) of induced DSB at MAT
416 locus. Homothallic endonuclease (HO) cutting efficiency at MAT locus was calculated using qPCR
417 with primer pair spanning the HO cut site normalized to uncut control site, interV (long intergenic
418 region on chromosome V). A similar qPCR approach normalized to a control site is also used to
419 directly measure resection on each side of the HO break, progressive loss of one strand
420 decreasing by up to 2-fold the amount of template at different distance from the break. Primer
421 sequences are available upon request. Antibodies used for ChIP are as follows: anti-Eaf1 [7], anti-
422 Rfa1 (Agrisera AS 07214), anti-Rad51(Santa Cruz y-180), anti-Rad52(Santa Cruz yC-17).

423 **Recombinant protein purification and pull-down assay**

424 Recombinant proteins were purified from BL-21 bacteria using standard protocol described
425 previously [73]. In brief, bacterial culture was growth overnight at 16°C in presence of IPTG.
426 Bacterial pellet was treated with lysozyme and sonicated. Soluble fraction was incubated with Ni-
427 nitrilotriacetic acid (NTA)-agarose (Qiagen) beads or glutathione-sepharose (GE Healthcare) for
428 3-4 hours on wheel at 4°C for His- or GST-tagged proteins respectively. Coomassie blue staining
429 was performed to estimate purified protein concentration with known bovine serum albumin
430 (BSA) standards. After elution ~300-600 ng of His-tagged protein were pre-cleared with
431 glutathione sepharose beads and incubated with immobilized GST-tagged protein in binding
432 buffer (25 mM HEPES [pH 7.5], 100 mM NaCl, 10% glycerol, 100 μg/ml BSA, 1 mM PMSF, 0.5 mM
433 dithiothreitol [DTT], 0.1% Tween 20, and protease inhibitors) at 4°C for 3 hours followed by
434 washing the beads three times. 1 μg of GST only immobilized protein was used as control. After

435 washing Laemmli buffer 1X was added followed by boiling and loading on SDS-PAGE for
436 visualization by western blotting using anti-His (Clonetech 631212) and anti-GST (Sigma G1160)
437 antibodies.

438 **Purification of acetylated Nej1 for mass spectrometry**

439 GST-tagged Nej1 was purified from wild-type and *esa1-L254P* (ts) background, followed by mass
440 spectrometry analysis to identify the acetylation sites as described previously with few
441 modifications [17]. In short, cells were grown in SC-Ura containing 2% raffinose till OD_{600} ~0.8-
442 1.0. Galactose (2% final) was added for the induction of the GST-tagged Nej1 (expressed from a
443 high-copy 2 micron vector) and cells were grown at 37°C for two additional hours. Cells were
444 harvested and lysed in extraction buffer (10mM Tris-HCl pH 8.0, 350mM NaCl, 0.1% NP-40, 10%
445 glycerol, 1mM DTT, 1mM PMSF, 2 µg/mL leupeptin, 2 µg/mL pepstatin A, 5 µg/mL aprotinin, 5
446 mM β-glycerophosphate, 10 mM sodium butyrate, 5 mM NaF, 10mM nicotinamide, 15µM TSA).
447 The lysate was centrifuged at 10,000g for 30min at 4°C, followed by ultracentrifugation for 1 hour
448 at 45,000g. The supernatant was precleared with CL6B beads (Sigma) before the addition of
449 glutathione-sepharose beads (GE Healthcare) for 3 hours on wheel at 4°C. After binding the
450 glutathione-sepharose beads were washed 5 times with wash buffer (20mM Hepes pH7.5,
451 200mM NaCl, 10mM sodium butyrate). Beads were mixed with elution buffer (50mM Tris-HCl
452 pH8.0, 10mM glutathione, 10% glycerol, 5mM sodium butyrate) at 4°C on wheel and first elution
453 was collected after 1 hour and other after overnight incubation. Next, protein A-sepharose beads
454 were washed with IP lysis buffer (75mM Tris-HCl ph 7.5, 50mM NaCl, 1mM EDTA, 1mM EGTA,
455 10% glycerol, 1% Tween-20, 1mM DTT, 1mM PMSF, 5mM NaF, 2 µg/mL leupeptin, 2 µg/mL
456 pepstatin A, 5 µg/mL aprotinin, 10mM sodium butyrate, 10mM, nicotinamide, 15µM TSA, 1 µM

457 MG132) and conjugated with 6µl of mouse monoclonal anti-acetylated-lysine (Cell Signalling
458 9681S). Antibody conjugated protein A-sepharose beads were incubated with GST elution at 4°C
459 for 3 hours on a wheel. After washing 4 times with IP wash buffer (50mM Hepes pH 7.0, 100mM
460 NaCl, 10 mM sodium butyrate) 20 µl of SDS-PAGE sample buffer was added and boiled. The
461 samples were resolved by SDS-PAGE followed by colloidal Coomassie blue staining to visualize
462 and cut gel bands, which were send for mass spectrometry analysis after trypsin digestion (Y.
463 Zhao lab, Univ. of Chicago). Peptide coverage obtained was 77% for the WT sample and 83% for
464 the mutant. List of confidently identified peptides containing an acetylated lysine residue is
465 presented in **S2 Table**.

466 **Chromatin binding and acetyltransferase assays**

467 Histone acetyltransferase assay was performed as described [9, 74]. 500ng of short
468 oligonucleosomes purified from methyl methanesulfonate MMS (0.05%) treated yeast cells, was
469 incubated with recombinant Rad9 at 30°C for 30 min. This was followed by the addition of
470 purified NuA4 complex (23) and 0.125 µCi of [^{3}H]acetyl coenzyme A ([3H]acetyl-CoA) in HAT
471 buffer (50 mM Tris-HCl [pH 8], 50 mM KCl plus NaCl, 0.1 mM EDTA, 5% glycerol, 1 mM DTT, 1 mM
472 PMSF and 20 mM sodium butyrate) at 30°C for 30 min. The reaction mixture was spotted on p81
473 filter paper, washed and air dried. The incorporation of radiolabeled acetylation was measured
474 by scintillation counting. For in-gel assay with recombinant GST-Nej1, reactions with NuA4 were
475 stopped in 1X Laemmli buffer, boiled and loaded on a 10% SDS-PAGE. Gel was treated with
476 En3hance (Perkin Elmer), dried and exposed on film.

477 **Non-homologous end joining (NHEJ) assay**

478 Plasmid re-ligation assay was performed as described [50]. 0.4 μg plasmid pSO98 supercoiled or
479 EcoR1 digested was used to transform *nej1*Δ yeast strains that harbored wild type or mutant
480 form of the *NEJ1* gene on a CEN:ARS low copy number plasmid. The transformed yeast was plated
481 on SC-His-Leu and SC-His-Ura and kept at 30°C. After 3 days colonies were counted and ratio of
482 colonies transformed with digested plasmid to undigested supercoiled plasmid was taken. Data
483 represents two independent biological replicates and error bar denotes the range between the
484 biological replicates.

485 Chromosomal NHEJ assay was performed as described [51]. Yeast background used
486 carries deletion of *HML* and *HMR* and galactose-inducible HO endonuclease that creates a single
487 DSB at the *MAT* locus. Endogenous *NEJ1* gene was deleted and wild type or mutant form of the
488 *NEJ1* gene was expressed from a low copy number CEN:ARS plasmid. The yeast cells were grown
489 overnight in YP-Raffinose media. Next day appropriate number of cells in the log phase were
490 plated on YP-Galactose and YP-Glucose plates and kept at 30°C. After 3-4 days the number of
491 colonies was quantified and ratio of colonies on YP-Galactose to YP-Glucose was calculated. Data
492 are from three independent biological replicates and error bar denotes the standard deviation
493 between the replicates.

494 **Acetyl-lysine immunoprecipitation**

495 Immunoprecipitation was performed as described previously (Cheng *et al.*, 2018). Cells were
496 grown in YPD till OD600 was ~0.5 followed by rapamycin addition (1μg/ml final) for 30 mins. MMS
497 (0.05%) or DMSO was added for 2 hours. Cells were collected and lysed in 10 mM Tris-HCl pH 8.0,
498 150 mM NaCl, 10% glycerol, 0.1% NP-40, 2 μg/mL leupeptin, 2 μg/mL pepstatin A, 5 μg/mL
499 aprotinin, 1 mM PMSF, 10 mM β-glycerophosphate, 1 mM Sodium Butyrate, 0.5 mM NaF, and 1

500 mM DTT. 4 µg of WCE was incubated with anti-acetyl (ImmuneChem ICP0380), overnight at 4°C.
501 Protein G Dynabeads (Invitrogen 10004D) was added to the reaction and kept on wheel at 4°C
502 for 4 additional hours. The IPs were washed and 1X Laemmli buffer was added and boiled. The
503 samples were resolved on SDS-PAGE followed by western blotting and analyzed with anti-Myc
504 (9E10 Babco MMS150R) and anti-Pgk1 (Abcam 113687).
505

506 ## Acknowledgments

507 We thank Olivier Jobin-Robitaille pour early work on this project, Zhiyou Deng and Yingming Zhao
508 (U. of Chicago) for mass spectrometry analysis of purified GST-Nej1. We thank James E. Haber
509 and Jennifer Cobbs for stimulating discussions. We are grateful to James E. Haber and Lorraine S.
510 Symington for providing strains and plasmids.
511

512 ## Author contributions

513 SA, VC, XC, GB, VS and MA performed experiments. SA and JC designed experiments, analyzed
514 the data and prepared the manuscript.

515 **Conflict of interest**

516 The authors declare that they have no conflict of interest.
517
518

519 ## References

520 1. Hanahan D, Weinberg Robert A. Hallmarks of Cancer: The Next Generation. Cell.
521 2011;144(5):646-74. doi: 10.1016/j.cell.2011.02.013.

522 2. Jackson SP, Bartek J. The DNA-damage response in human biology and disease. Nature.
523 2009;461(7267):1071-8. doi: 10.1038/nature08467.
524 3. Symington LS. Mechanism and regulation of DNA end resection in eukaryotes. Critical
525 Reviews in Biochemistry and Molecular Biology. 2016;51(3):195-212. doi:
526 10.3109/10409238.2016.1172552.
527 4. Chiruvella KK, Liang Z, Wilson TE. Repair of Double-Strand Breaks by End Joining. Cold
528 Spring Harbor Perspectives in Biology. 2013;5(5). doi: 10.1101/cshperspect.a012757.
529 5. Ceccaldi R, Rondinelli B, D'Andrea AD. Repair Pathway Choices and Consequences at the
530 Double-Strand Break. Trends in cell biology. 2016;26(1):52-64. Epub 2015/10/01. doi:
531 10.1016/j.tcb.2015.07.009. PubMed PMID: 26437586.
532 6. Bhargava R, Onyango DO, Stark JM. Regulation of Single-Strand Annealing and its Role in
533 Genome Maintenance. Trends in genetics : TIG. 2016;32(9):566-75. Epub 2016/07/19. doi:
534 10.1016/j.tig.2016.06.007. PubMed PMID: 27450436.
535 7. Auger A, Galarneau L, Altaf M, Nourani A, Doyon Y, Utley RT, et al. Eaf1 Is the Platform for
536 NuA4 Molecular Assembly That Evolutionarily Links Chromatin Acetylation to ATP-Dependent
537 Exchange of Histone H2A Variants. Molecular and Cellular Biology. 2008;28(7):2257-70. doi:
538 10.1128/mcb.01755-07.
539 8. Doyon Y, Selleck W, Lane WS, Tan S, Côté J. Structural and Functional Conservation of the
540 NuA4 Histone Acetyltransferase Complex from Yeast to Humans. Molecular and Cellular Biology.
541 2004;24(5):1884-96. doi: 10.1128/mcb.24.5.1884-1896.2004.
542 9. Allard S, Utley RT, Savard J, Clarke A, Grant P, Brandl CJ, et al. NuA4, an essential
543 transcription adaptor/histone H4 acetyltransferase complex containing Esa1p and the ATM-
544 related cofactor Tra1p. The EMBO Journal. 1999;18(18):5108-19. doi:
545 10.1093/emboj/18.18.5108.
546 10. Clarke AS, Lowell JE, Jacobson SJ, Pillus L. Esa1p Is an Essential Histone Acetyltransferase
547 Required for Cell Cycle Progression. Molecular and Cellular Biology. 1999;19(4):2515-26. doi:
548 10.1128/mcb.19.4.2515.
549 11. Steunou A-L, Rossetto D, Côté J. Regulating Chromatin by Histone Acetylation. In:
550 Workman JL, Abmayr SM, editors. Fundamentals of Chromatin. New York, NY: Springer New York;
551 2014. p. 147-212.
552 12. Keogh M-C, Mennella TA, Sawa C, Berthelet S, Krogan NJ, Wolek A, et al. The
553 Saccharomyces cerevisiae histone H2A variant Htz1 is acetylated by NuA4. Genes &
554 Development. 2006;20(6):660-5. doi: 10.1101/gad.1388106.
555 13. Soria G, Polo Sophie E, Almouzni G. Prime, Repair, Restore: The Active Role of Chromatin
556 in the DNA Damage Response. Molecular Cell. 2012;46(6):722-34. doi:
557 https://doi.org/10.1016/j.molcel.2012.06.002.
558 14. Doyon Y, Côté J. The highly conserved and multifunctional NuA4 HAT complex. Current
559 Opinion in Genetics & Development. 2004;14(2):147-54. doi:
560 https://doi.org/10.1016/j.gde.2004.02.009.
561 15. Rossetto D, Cramet M, Wang AY, Steunou A-L, Lacoste N, Schulze JM, et al. Eaf5/7/3 form
562 a functionally independent NuA4 submodule linked to RNA polymerase II-coupled nucleosome
563 recycling. The EMBO Journal. 2014;33(12):1397-415. doi: 10.15252/embj.201386433.

564 16. Yi C, Ma M, Ran L, Zheng J, Tong J, Zhu J, et al. Function and Molecular Mechanism of
565 Acetylation in Autophagy Regulation. Science. 2012;336(6080):474-7. doi:
566 10.1126/science.1216990.
567 17. Lin Y-y, Lu J-y, Zhang J, Walter W, Dang W, Wan J, et al. Protein Acetylation Microarray
568 Reveals that NuA4 Controls Key Metabolic Target Regulating Gluconeogenesis. Cell.
569 2009;136(6):1073-84. doi: 10.1016/j.cell.2009.01.033.
570 18. Choy JS, Kron SJ. NuA4 Subunit Yng2 Function in Intra-S-Phase DNA Damage Response.
571 Molecular and Cellular Biology. 2002;22(23):8215-25. doi: 10.1128/mcb.22.23.8215-8225.2002.
572 19. Bird AW, Yu DY, Pray-Grant MG, Qiu Q, Harmon KE, Megee PC, et al. Acetylation of histone
573 H4 by Esa1 is required for DNA double-strand break repair. Nature. 2002;419(6905):411-5. doi:
574 10.1038/nature01035.
575 20. Downs JA, Allard S, Jobin-Robitaille O, Javaheri A, Auger A, Bouchard N, et al. Binding of
576 Chromatin-Modifying Activities to Phosphorylated Histone H2A at DNA Damage Sites. Molecular
577 Cell. 2004;16(6):979-90. doi: 10.1016/j.molcel.2004.12.003.
578 21. Bennett G, Peterson CL. SWI/SNF recruitment to a DNA double-strand break by the NuA4
579 and Gcn5 histone acetyltransferases. DNA Repair. 2015;30:38-45. doi:
580 https://doi.org/10.1016/j.dnarep.2015.03.006.
581 22. House Nealia CM, Yang Jiahui H, Walsh Stephen C, Moy Jonathan M, Freudenreich
582 Catherine H. NuA4 Initiates Dynamic Histone H4 Acetylation to Promote High-Fidelity Sister
583 Chromatid Recombination at Postreplication Gaps. Molecular Cell. 2014;55(6):818-28. doi:
584 10.1016/j.molcel.2014.07.007.
585 23. Cheng X, Jobin-Robitaille O, Billon P, Buisson R, Niu H, Lacoste N, et al. Phospho-
586 dependent recruitment of the yeast NuA4 acetyltransferase complex by MRX at DNA breaks
587 regulates RPA dynamics during resection. Proceedings of the National Academy of Sciences.
588 2018;115(40):10028-33. doi: 10.1073/pnas.1806513115.
589 24. Cheng X, Cote V, Cote J. NuA4 and SAGA acetyltransferase complexes cooperate for repair
590 of DNA breaks by homologous recombination. PLoS Genet. 2021;17(7):e1009459. Epub
591 2021/07/07. doi: 10.1371/journal.pgen.1009459. PubMed PMID: 34228704.
592 25. Javaheri A, Wysocki R, Jobin-Robitaille O, Altaf M, Côté J, Kron SJ. Yeast G1 DNA damage
593 checkpoint regulation by H2A phosphorylation is independent of chromatin remodeling.
594 Proceedings of the National Academy of Sciences. 2006;103(37):13771-6. doi:
595 10.1073/pnas.0511192103.
596 26. Jacquet K, Fradet-Turcotte A, Avvakumov N, Lambert J-P, Roques C, Pandita Raj K, et al.
597 The TIP60 Complex Regulates Bivalent Chromatin Recognition by 53BP1 through Direct H4K20me
598 Binding and H2AK15 Acetylation. Molecular Cell. 2016;62(3):409-21. doi:
599 10.1016/j.molcel.2016.03.031.
600 27. Tang J, Cho NW, Cui G, Manion EM, Shanbhag NM, Botuyan MV, et al. Acetylation limits
601 53BP1 association with damaged chromatin to promote homologous recombination. Nature
602 Structural & Molecular Biology. 2013;20(3):317-25. doi: 10.1038/nsmb.2499.
603 28. Dantuma NP, van Attikum H. Spatiotemporal regulation of posttranslational modifications
604 in the DNA damage response. The EMBO Journal. 2016;35(1):6-23. doi:
605 10.15252/embj.201592595.
606 29. Ferrari M, Dibitetto D, De Gregorio G, Eapen VV, Rawal CC, Lazzaro F, et al. Functional
607 Interplay between the 53BP1-Ortholog Rad9 and the Mre11 Complex Regulates Resection, End-

608 Tethering and Repair of a Double-Strand Break. PLOS Genetics. 2015;11(1):e1004928. doi:
609 10.1371/journal.pgen.1004928.
610 30. Escribano-Díaz C, Orthwein A, Fradet-Turcotte A, Xing M, Young Jordan TF, Tkáč J, et al. A
611 Cell Cycle-Dependent Regulatory Circuit Composed of 53BP1-RIF1 and BRCA1-CtIP Controls DNA
612 Repair Pathway Choice. Molecular Cell. 2013;49(5):872-83. doi: 10.1016/j.molcel.2013.01.001.
613 31. Noordermeer SM, Adam S, Setiaputra D, Barazas M, Pettitt SJ, Ling AK, et al. The shieldin
614 complex mediates 53BP1-dependent DNA repair. Nature. 2018;560(7716):117-21. doi:
615 10.1038/s41586-018-0340-7.
616 32. Zimmermann M, Lottersberger F, Buonomo SB, Sfeir A, de Lange T. 53BP1 Regulates DSB
617 Repair Using Rif1 to Control 5′ End Resection. Science. 2013;339(6120):700-4. doi:
618 10.1126/science.1231573.
619 33. Grenon M, Costelloe T, Jimeno S, O'Shaughnessy A, FitzGerald J, Zgheib O, et al. Docking
620 onto chromatin via the Saccharomyces cerevisiae Rad9 Tudor domain. Yeast. 2007;24(2):105-19.
621 doi: 10.1002/yea.1441.
622 34. Hammet A, Magill C, Heierhorst J, Jackson SP. Rad9 BRCT domain interaction with
623 phosphorylated H2AX regulates the G1 checkpoint in budding yeast. EMBO reports.
624 2007;8(9):851-7. doi: 10.1038/sj.embor.7401036.
625 35. Wysocki R, Javaheri A, Allard S, Sha F, Côté J, Kron SJ. Role of Dot1-Dependent Histone H3
626 Methylation in G₁ and S Phase DNA Damage Checkpoint Functions of Rad9.
627 Molecular and Cellular Biology. 2005;25(19):8430-43. doi: 10.1128/mcb.25.19.8430-8443.2005.
628 36. Bennett G, Papamichos-Chronakis M, Peterson CL. DNA repair choice defines a common
629 pathway for recruitment of chromatin regulators. Nat Commun. 2013;4:2084. Epub 2013/07/03.
630 doi: 10.1038/ncomms3084. PubMed PMID: 23811932; PubMed Central PMCID: PMC3731036.
631 37. Trovesi C, Falcettoni M, Lucchini G, Clerici M, Longhese MP. Distinct Cdk1 Requirements
632 during Single-Strand Annealing, Noncrossover, and Crossover Recombination. PLOS Genetics.
633 2011;7(8):e1002263. doi: 10.1371/journal.pgen.1002263.
634 38. Abraham RT. Cell cycle checkpoint signaling through the ATM and ATR kinases. Genes &
635 Development. 2001;15(17):2177-96. doi: 10.1101/gad.914401.
636 39. Smith GCM, Jackson SP. The DNA-dependent protein kinase. Genes & Development.
637 1999;13(8):916-34.
638 40. Clerici M, Mantiero D, Guerini I, Lucchini G, Longhese MP. The Yku70–Yku80 complex
639 contributes to regulate double-strand break processing and checkpoint activation during the cell
640 cycle. EMBO reports. 2008;9(8):810-8. doi: 10.1038/embor.2008.121.
641 41. Tsukamoto Y, Mitsuoka C, Terasawa M, Ogawa H, Ogawa T. Xrs2p Regulates Mre11p
642 Translocation to the Nucleus and Plays a Role in Telomere Elongation and Meiotic
643 Recombination. Molecular Biology of the Cell. 2005;16(2):597-608. doi: 10.1091/mbc.e04-09-
644 0782. PubMed PMID: 15548595.
645 42. Oh J, Al-Zain A, Cannavo E, Cejka P, Symington Lorraine S. Xrs2 Dependent and
646 Independent Functions of the Mre11-Rad50 Complex. Molecular Cell. 2016;64(2):405-15. doi:
647 10.1016/j.molcel.2016.09.011.
648 43. Oh J, Lee SJ, Rothstein R, Symington LS. Xrs2 and Tel1 Independently Contribute to MR-
649 Mediated DNA Tethering and Replisome Stability. Cell Rep. 2018;25(7):1681-92 e4. Epub
650 2018/11/15. doi: 10.1016/j.celrep.2018.10.030. PubMed PMID: 30428339; PubMed Central
651 PMCID: PMC6317890.

652 44. Zou L, Elledge SJ. Sensing DNA Damage Through ATRIP Recognition of RPA-ssDNA
653 Complexes. Science. 2003;300(5625):1542-8. doi: 10.1126/science.1083430.
654 45. Gobbini E, Cesena D, Galbiati A, Lockhart A, Longhese MP. Interplays between ATM/Tel1
655 and ATR/Mec1 in sensing and signaling DNA double-strand breaks. DNA Repair. 2013;12(10):791-
656 9. doi: https://doi.org/10.1016/j.dnarep.2013.07.009.
657 46. Paciotti V, Clerici M, Lucchini G, Longhese MP. The checkpoint protein Ddc2, functionally
658 related to S. pombe Rad26, interacts with Mec1 and is regulated by Mec1-dependent
659 phosphorylation in budding yeast. Genes & Development. 2000;14(16):2046-59. doi:
660 10.1101/gad.14.16.2046.
661 47. Ivanov EL, Sugawara N, Fishman-Lobell J, Haber JE. Genetic Requirements for the Single-
662 Strand Annealing Pathway of Double-Strand Break Repair in Saccharomyces
663 cerevisiae. Genetics. 1996;142(3):693-704.
664 48. Zhang Y, Hefferin ML, Chen L, Shim EY, Tseng H-M, Kwon Y, et al. Role of Dnl4–Lif1 in
665 nonhomologous end-joining repair complex assembly and suppression of homologous
666 recombination. Nature Structural & Molecular Biology. 2007;14(7):639-46. doi:
667 10.1038/nsmb1261.
668 49. Jain S, Sugawara N, Haber JE. Role of Double-Strand Break End-Tethering during Gene
669 Conversion in Saccharomyces cerevisiae. PLoS Genet. 2016;12(4):e1005976. Epub 2016/04/14.
670 doi: 10.1371/journal.pgen.1005976. PubMed PMID: 27074148; PubMed Central PMCID:
671 PMC4830573.
672 50. Ooi SL, Shoemaker DD, Boeke JD. A DNA Microarray-Based Genetic Screen for
673 Nonhomologous End-Joining Mutants in Saccharomyces cerevisiae. Science.
674 2001;294(5551):2552-6. doi: 10.1126/science.1065672.
675 51. Valencia M, Bentele M, Vaze MB, Herrmann G, Kraus E, Lee SE, et al. NEJ1 controls non-
676 homologous end joining in Saccharomyces cerevisiae. Nature. 2001;414(6864):666-9. doi:
677 10.1038/414666a.
678 52. Chang HHY, Pannunzio NR, Adachi N, Lieber MR. Non-homologous DNA end joining and
679 alternative pathways to double-strand break repair. Nature Reviews Molecular Cell Biology.
680 2017;18(8):495-506. doi: 10.1038/nrm.2017.48.
681 53. Kegel A, Sjöstrand JOO, Åström SU. Nej1p, a cell type-specific regulator of
682 nonhomologous end joining in yeast. Current Biology. 2001;11(20):1611-7. doi:
683 https://doi.org/10.1016/S0960-9822(01)00488-2.
684 54. Deshpande RA, Wilson TE. Modes of interaction among yeast Nej1, Lif1 and Dnl4 proteins
685 and comparison to human XLF, XRCC4 and Lig4. DNA repair. 2007;6(10):1507-16. Epub
686 2007/06/12. doi: 10.1016/j.dnarep.2007.04.014. PubMed PMID: 17567543.
687 55. Sulek M, Yarrington R, McGibbon G, Boeke JD, Junop M. A critical role for the C-terminus
688 of Nej1 protein in Lif1p association, DNA binding and non-homologous end-joining. DNA Repair.
689 2007;6(12):1805-18. doi: https://doi.org/10.1016/j.dnarep.2007.07.009.
690 56. Mahaney BL, Lees-Miller SP, Cobb JA. The C-terminus of Nej1 is critical for nuclear
691 localization and non-homologous end-joining. DNA Repair. 2014;14:9-16. doi:
692 https://doi.org/10.1016/j.dnarep.2013.12.002.
693 57. Chen X, Tomkinson AE. Yeast Nej1 Is a Key Participant in the Initial End Binding and Final
694 Ligation Steps of Nonhomologous End Joining. Journal of Biological Chemistry. 2011;286(6):4931-
695 40. doi: 10.1074/jbc.M110.195024.

696 58. Reid DA, Keegan S, Leo-Macias A, Watanabe G, Strande NT, Chang HH, et al. Organization
697 and dynamics of the nonhomologous end-joining machinery during DNA double-strand break
698 repair. Proceedings of the National Academy of Sciences. 2015;112(20):E2575-E84. doi:
699 10.1073/pnas.1420115112.
700 59. Graham TGW, Carney SM, Walter JC, Loparo JJ. A single XLF dimer bridges DNA ends
701 during nonhomologous end joining. Nature Structural & Molecular Biology. 2018;25(9):877-84.
702 doi: 10.1038/s41594-018-0120-y.
703 60. Mojumdar A, Sorenson K, Hohl M, Toulouze M, Lees-Miller SP, Dubrana K, et al. Nej1
704 Interacts with Mre11 to Regulate Tethering and Dna2 Binding at DNA Double-Strand Breaks. Cell
705 Reports. 2019;28(6):1564-73.e3. doi: https://doi.org/10.1016/j.celrep.2019.07.018.
706 61. Sorenson KS, Mahaney BL, Lees-Miller SP, Cobb JA. The non-homologous end-joining
707 factor Nej1 inhibits resection mediated by Dna2–Sgs1 nuclease-helicase at DNA double strand
708 breaks. Journal of Biological Chemistry. 2017;292(35):14576-86. doi: 10.1074/jbc.M117.796011.
709 62. Ahnesorg P, Jackson SP. The non-homologous end-joining protein Nej1p is a target of the
710 DNA damage checkpoint. DNA Repair. 2007;6(2):190-201. doi:
711 https://doi.org/10.1016/j.dnarep.2006.09.010.
712 63. Haruki H, Nishikawa J, Laemmli UK. The Anchor-Away Technique: Rapid, Conditional
713 Establishment of Yeast Mutant Phenotypes. Molecular Cell. 2008;31(6):925-32. doi:
714 10.1016/j.molcel.2008.07.020.
715 64. Kollenstart L, de Groot AJL, Janssen GMC, Cheng X, Vreeken K, Martino F, et al. Gcn5 and
716 Esa1 function as histone crotonyltransferases to regulate crotonylation-dependent transcription.
717 Journal of Biological Chemistry. 2019;294(52):20122-34. doi: 10.1074/jbc.RA119.010302.
718 65. Cohen HY, Lavu S, Bitterman KJ, Hekking B, Imahiyerobo TA, Miller C, et al. Acetylation of
719 the C Terminus of Ku70 by CBP and PCAF Controls Bax-Mediated Apoptosis. Molecular Cell.
720 2004;13(5):627-38. doi: https://doi.org/10.1016/S1097-2765(04)00094-2.
721 66. Li S, Shi B, Liu X, An H-X. Acetylation and Deacetylation of DNA Repair Proteins in Cancers.
722 Frontiers in Oncology. 2020;10(2184). doi: 10.3389/fonc.2020.573502.
723 67. Harrison JC, Haber JE. Surviving the Breakup: The DNA Damage Checkpoint. Annual
724 Review of Genetics. 2006;40(1):209-35. doi: 10.1146/annurev.genet.40.051206.105231.
725 PubMed PMID: 16805667.
726 68. Orthwein A, Noordermeer SM, Wilson MD, Landry S, Enchev RI, Sherker A, et al. A
727 mechanism for the suppression of homologous recombination in G1 cells. Nature.
728 2015;528(7582):422-6. doi: 10.1038/nature16142.
729 69. Jeong J, Juhn K, Lee H, Kim S-H, Min B-H, Lee K-M, et al. SIRT1 promotes DNA repair activity
730 and deacetylation of Ku70. Experimental & Molecular Medicine. 2007;39(1):8-13. doi:
731 10.1038/emm.2007.2.
732 70. Miller KM, Tjeertes JV, Coates J, Legube G, Polo SE, Britton S, et al. Human HDAC1 and
733 HDAC2 function in the DNA-damage response to promote DNA nonhomologous end-joining.
734 Nature Structural & Molecular Biology. 2010;17(9):1144-51. doi: 10.1038/nsmb.1899.
735 71. Boulton SJ, Jackson SP. Components of the Ku-dependent non-homologous end-joining
736 pathway are involved in telomeric length maintenance and telomeric silencing. The EMBO
737 Journal. 1998;17(6):1819-28. doi: 10.1093/emboj/17.6.1819.
738 72. Guo X, Bai Y, Zhao M, Zhou M, Shen Q, Yun CH, et al. Acetylation of 53BP1 dictates the
739 DNA double strand break repair pathway. Nucleic acids research. 2018;46(2):689-703. Epub

740 2017/12/01. doi: 10.1093/nar/gkx1208. PubMed PMID: 29190394; PubMed Central PMCID:
741 PMC5778472.
742 73. Setiaputra D, Ahmad S, Dalwadi U, Steunou A-L, Lu S, Ross JD, et al. Molecular
743 Architecture of the Essential Yeast Histone Acetyltransferase Complex NuA4 Redefines Its
744 Multimodularity. Molecular and Cellular Biology. 2018;38(9):e00570-17. doi:
745 10.1128/mcb.00570-17.
746 74. Steunou A-L, Cramet M, Rossetto D, Aristizabal MJ, Lacoste N, Drouin S, et al. Combined
747 Action of Histone Reader Modules Regulates NuA4 Local Acetyltransferase Function but Not Its
748 Recruitment on the Genome. Molecular and Cellular Biology. 2016;36(22):2768-81. doi:
749 10.1128/mcb.00112-16.
750 75. Lee SE, Moore JK, Holmes A, Umezu K, Kolodner RD, Haber JE. Saccharomyces Ku70,
751 Mre11/Rad50, and RPA Proteins Regulate Adaptation to G2/M Arrest after DNA Damage. Cell.
752 1998;94(3):399-409. doi: https://doi.org/10.1016/S0092-8674(00)81482-8.

753

754

755 **FIGURE LEGENDS:**

756 **Fig 1: NHEJ factors inhibit NuA4 recruitment and end resection at a DSB in G1.**

757 (A) Schematic representation of the experiment in (B). Wild type Rad9 binds to chromatin and
758 inhibits NuA4 from acetylating histones, whereas Rad9 mutants are unable to bind chromatin
759 efficiently, thus resulting in acetylation of histones by NuA4.

760 (B) *In vitro* HAT assay showing inhibition of NuA4 acetyltransferase activity by Rad9 using yeast
761 native chromatin purified from MMS-treated cells and recombinant Rad9 (wild type, tudor-
762 Y798Q and BRCT- K1088E domain mutant, S1A Fig). Recombinant Rad9 wild type and mutants
763 were incubated with 500ng of chromatin. Afterwards NuA4 was added along with ^{3}H-acetyl-CoA
764 followed by spotting on P81 membrane and scintillation counting. Error bars indicate the ranges
765 of duplicate reactions. Only 0.5ug of WT and tudor mutant show a statistically significant
766 decrease of acetylation compared to control (BSA). Higher amount of Rad9 leads to more
767 inhibition (S1B Fig).

768 (C-H) ChIP-qPCR showing increased recruitment of NuA4 (Eaf1 subunit) and Rfa1 (RPA) in *rad9*Δ
769 (C-D)*, yku80*Δ, y*ku80*Δ*rad9*Δ (E-F) and *nej1*Δ (G-H) compared to wild type at an HO-induced DSB
770 in G1. ChIP-qPCR analysis was performed using Eaf1 and Rfa1 antibodies. Cells with *bar1*Δ
771 background were synchronized in G1 phase using α-factor for 6 hours in YP-Raffinose followed
772 by addition of galactose for 3 hours to induce DSB. The data represents two independent
773 biological replicates and error bar denotes range between the replicates. Yeast strains used had
774 similar HO cutting efficiency (S1E-I Fig)

775

776 **Fig 2: Xrs2-dependent recruitment of NuA4 at a DSB in G1.**

777 (A-D) ChIP-qPCR of Rfa1 and Eaf1 shows loss of NuA4 (A, C) and resection (B, D) in *xrs2*Δ,
778 *xrs2*Δ*rad9*Δ and *xrs2*Δ*rad9*Δy*ku80*Δ compared to wild type at HO-induced DSB in G1 synchronized
779 cells. See also S2D Fig for direct measurement of DNA end resection by qPCR.
780 (E-F) ChIP-qPCR in the *mre11-H125N* mutant strain shows decreased resection but unaffected
781 NuA4 recruitment compared to wild type in G1 cells. ChIP-qPCR was performed as described in
782 (Fig 1). Yeast strains used showed similar HO cutting efficiency (S2A-C Fig).
783
784 **Fig 3: Alternate mode of NuA4 recruitment in G1 in conditions of Xrs2 functional bypass.**
785 (A-B) Resection and NuA4 recruitment is partially restored in the *xrs2*Δ *rad9*Δy*ku80*Δ background
786 with expression of Mre11-NLS from a low copy number ARS:CEN plasmid. ChIP-qPCR of Eaf1 and
787 Rfa1 was performed as in (Fig 1) in cells synchronized in G1.
788 (C-D) Resection and NuA4 recruitment is largely restored in *xrs2*Δ *rad9*Δy*ku80*Δ background by
789 expression of Mre11-NLS-X85 that more fully bypasses Xrs2 functions.
790 (E-F) Expression of Mre11-NLS also partially rescues NuA4 recruitment and resection (Rfa1 signal)
791 in the *xrs2*Δ background in asynchronous cells (on the left side proximal to the DSB site).
792 (See S3 Fig for *xrs2Δ* phenotypic suppression by Mre11-NLS and HO-cutting efficiencies)
793
794 **Fig 4: The alternate mode of NuA4 recruitment at the DSB is Lcd1/Ddc2-dependent.**
795 (A-B) Resection and NuA4 recruitment can be further rescued in the *xrs2Δ* background by
796 expressing Mre11-NLS along catalytically active Exo1. End resection is directly measured by
797 decreased DNA signal near the break and NuA4 recruitment is monitored as before. Expression
798 of a catalytically dead Exo1 is used as control (Exo1-D173A).

799 (C-D) Resection is also rescued in the *lcd1*Δ*xrs2*Δ background with *pMRE11-NLS* and
800 overexpression of Exo1-WT but not Exo1-D173A mutant, but this is not the case for NuA4
801 recruitment. NuA4 signal does not show a resection-correlated increase with Exo1-WT compared
802 to the Exo1-D173A mutant or the empty vector.
803 Resection is presented as % of Intact DNA determined by qPCR on genomic DNA at indicated sites
804 and normalized to the negative control intergenic V. Cells were grown in YP-Raff till early log
805 phase followed by addition of galactose for 3 hours to induce the DSB. Yeast strains used had
806 similar HO cutting efficiency (S4C-D Fig).
807
808 **Fig 5: Decreased hyper-resection in a NuA4 acetylation defective mutant in G1 and defect in**
809 **DNA break repair by SSA.**
810 (A-B) ChIP-qPCR of Rad52 around the HO-induced DSB in G1 blocked cells. *rad9*Δy*ku80*Δ, y*ku80*Δ
811 (A) and *nej1*Δ (B) show higher recruitment of Rad52 compared to wild type conditions.
812 (C) Reduced histone H4 acetylation in the *esa1-ts* background at semi-restrictive temperature.
813 Western blot analysis of WCE from yeast strains used for ChIP-qPCR in (D). Samples were
814 collected before addition of α-factor at permissive temperature (23°C) in YP-Raff. α-factor was
815 added and cultures were moved to semi-restrictive temperature (32°C) followed by addition of
816 galactose to induced the HO cut for 3 hours.
817 (D) ChIP-qPCR of Rfa1 around the HO-induced DSB in G1 cells showing reduced resection in the
818 *rad9Δyku80Δ* background with the introduction of the NuA4 *esa1-ts* defective allele. Yeast strains
819 used had similar HO cutting efficiency (S5C Fig).

820 (E) The sensitivity of the *esa1-ts* mutant cells to DNA damage is partially suppressed by deletion
821 of core NHEJ factors. 10-fold serial dilution spot assays were performed with *esa1-L254P*,
822 *rad9*Δy*ku80*Δ and *rad9*Δy*ku80*Δ*esa1-L254P* cells in the absence or the presence of DNA damaging
823 agent MMS.
824 (F) The *esa1-ts* mutation leads to a decrease of DSB repair by resection-based single-strand
825 annealing. A yeast strain with direct repeats 20kb apart is used as reporter for SSA efficiency. In
826 the absence of Rad51 the DSN induced by HO between the repeats is mostly repaired by SSA with
827 Rad52. Efficiency of repair is monitored by survival with 10-fold dilution spot assays in conditions
828 of *GAL-HO* induction or not.
829
830 **Fig 6: NuA4 inhibits NHEJ through acetylation of Nej1.**
831 (A) *in vitro* acetylation assay using purified NuA4 complex and recombinant GST-Nej1. After the
832 reaction with radioactive acetyl-CoA, the reactions were loaded on gel, processed for
833 fluorography/exposed on film. The GST-Nej1 protein is clearly acetylated by NuA4 *in vitro*.GST
834 alone is used as negative control. Faint labeled bands in both samples correspond to known auto-
835 acetylation of NuA4 subunits (e.g. Yng2 at 36kDa [17]).
836 (B) Nej1 is acetylated *in vivo.* Anti-acetyl-lysine immunoprecipitations were performed on
837 extracts from cells over-expressing GST-NEJ1 from a multicopy vector. Nej1 Acetylation level is
838 detected by anti-GST western on the immunoprecipitated material.
839 (C) Drawing showing the locations of the acetylated residues identified by mass spectrometry
840 that were not present in the *esa1-ts* sample (see also S6A Fig and S2 Table for full list of identified
841 acetylated peptides). Known functional domains of Nej1 are also indicated.

842 (D) Western blot on whole cell extracts comparing native wild type and mutant Nej1 expression
843 levels in constructed strains used in (E).
844 (E) *nej1-3KR* and *nej1-3KQ* mutant cells show reduced plasmid re-ligation efficiency for EcoR1
845 linearized pSO98 plasmid. Samples were normalized to wild type, which was set at 100%.
846 (F-G) Increased NuA4 and resection/RPA recruitment in the *nej1-3KQ* mutant compared to wild
847 type *NEJ1* and the *nej1-3KR* mutant background. ChIP-qPCR using anti-Eaf1 (F) and anti-Rfa1 (G)
848 antibodies in G1 synchronized cells as described in Fig 1. Yeast strains used showed similar HO
849 cutting efficiency (S6C Fig).
850 (H) GST pull-down with recombinant proteins. Recombinant Nej1-3KQ shows reduced interaction
851 with rYku80 compared to Nej1-WT and Nej1-3KR. rNej1 is GST tagged for pull-down whereas
852 rKu80 is 6XHis tagged for detection by western. Empty GST was used as negative control.
853 (I) GST pull-down as in (H). Recombinant Nej1-3KQ and Nej1-3KR show reduced interaction with
854 rLif1 compared to wild type Nej1. rLif1 is 6XHis tagged. Empty GST was used as negative control.
855 (J) Yku80 is acetylated on lysine residues *in vivo* in a NuA4-dependent manner. Acetyl-lysine
856 immunoprecipitation in an Esa1-FRB anchor-away[24]/Yku80-13myc background shows much
857 reduced signal for Yku80 after the rapamycin treatment that depletes Esa1 from the nucleus. The
858 effect of DNA damage was also monitored by treating the cells with MMS. Pgk1 was used as
859 loading control. The efficiency of Esa1 depletion was monitored by western blot showing loss of
860 H4 acetylation (S6G Fig).
861
862 **Fig 7: Reciprocal antagonism between the NuA4 complex and the NHEJ machinery: a central**
863 **regulatory mechanism for repair pathway choice.**

864 Model: While chromatin-bound Rad9 can inhibit NuA4 recruitment and chromatin acetylation to
865 favor repair by NHEJ, recruitment of NuA4 by MRX can lead to acetylation of NHEJ core factors
866 like Nej1 and Yku80. This perturbs the interactions between NHEJ factors, inhibiting NHEJ and
867 enabling resection of DNA ends. As resection produces ssDNA, NuA4 spreads on each side of the
868 break, favoring resection-based repair pathways like HR and SSA. The possible alternate mode of
869 NuA4 recruitment by Lcd1/Ddc2 in specific conditions is also depicted. "Ac" represents
870 acetylation performed by NuA4.
871
872

873 **Supporting Information:**

874 **S1 Fig. Inhibition of NuA4 by Rad9 in vitro but no inhibition of NuA4 and resection spreading**
875 **by NHEJ factors in asynchronous cells.** Related to Fig 1.

876 (A) Purified recombinant Rad9 wild-type and mutants were resolved by SDS-PAGE and stained
877 with Coomassie blue stain. Known concentrations of BSA were used to estimate the
878 concentration of purified recombinant proteins using the ImageJ software.

879 (B) Inhibition of NuA4-dependent acetylation of chromatin by Rad9 in vitro. The assays was
880 performed as in Fig 1B but using more recombinant rad9 proteins. In these conditions the
881 difference between WT and mutant Rad9 is more subtle because of mass effect, but still visible
882 with 2ug.

883 (C) ChIP-qPCR showing NuA4 enrichment around HO DSB at the *MAT* locus in wild type and *rad9*Δ
884 in asynchronous cells.

885 (D) ChIP-qPCR with antibody against Rfa1 showing no difference in resection at the *MAT* locus
886 between wild type and *nej1*Δ in asynchronous cells.

887 (E-I) HO cutting efficiency at the *MAT* locus after 3 hours of galactose induction in wild type and,
888 *rad9*Δ in asynchronous cells (E), *rad9*Δ in G1 synchronized cells (F), y*ku80*Δ and y*ku80*Δ*rad9*Δ in
889 G1 synchronized cells (G), *nej1*Δ in G1 synchronized cells (H), *nej1*Δ in asynchronous cells (I).

890

891 **S2 Fig. Difference in NuA4 and resection signal seen between wild type and mutants not caused**
892 **by uneven HO cutting at *MAT* locus and a different method to measure DNA end resection in**
893 **parallel to ChIP-qPCR with Rfa1.**

894 (A-C) HO cutting efficiency at MAT locus in G1 synchronized cells after 3 hours of galactose
895 induction between wild type and, *xrs2*Δ*rad9*Δ (A), *xrs2*Δ*rad9*Δy*ku80*Δ (B), *mre11-H125N* (C).
896 (D) DNA end resection is directly measured by decreased DNA signal near the break in WT, *xrs2Δ,*
897 *yku80Δrad9Δ* and *xrs2Δrad9Δyku80Δ* backgrounds. Hyper resection phenotype is clearly seen
898 with *yku80/rad9* double mutant but disappear in the absence of Xrs2. Resection is presented as
899 % of Intact DNA determined by qPCR on genomic DNA at indicated sites and normalized to the
900 negative control intergenic V. Cells were grown in YP-Raff till early log phase followed by addition
901 of galactose for 3 hours to induce the DSB.
902
903 **S3 Fig. p*MRE11-NLS* suppresses defect of *xrs2*Δ.**
904 (A) Phenotypic analysis showing introduction of p*MRE11-NLS* suppresses the sensitivity of *xrs2*Δ
905 cells to the DNA damaging drug MMS. 10-fold serial dilutions of log phase cells were spotted on
906 synthetic complete -URA plates with and without MMS.
907 (B-D) HO cutting efficiency at *MAT* locus after 3 hours of galactose induction in the indicated
908 strains.
909
910 **S4 Fig. Lcd1/Ddc2 is not required for NuA4 recruitment or resection in asynchronous cells.**
911 (A-B) ChIP-qPCR showing that the *lcd1*Δ *xrs2*Δ background results in loss of RPA signal (A), and
912 NuA4 (B) at the HO induced DSB in asynchronous cells. The single mutant *lcd1*Δ (loss of Mec1)
913 does not affect resection but shows slightly less NuA4 signal compared to wild type close to the
914 break.

915 (C-D) HO cutting efficiency at *MAT* locus after 3 hours of galactose induction in the indicated
916 strains.
917
918 **S5 Fig. The *esa1-ts* allele does not affect the recruitment of recombination protein Rad52 in a**
919 **hyper resection background in G1.**
920 (A) ChIP-qPCR with a Rad51 antibody around the induced DSB at *MAT* locus in G1 synchronized
921 cells. y*ku80*Δ and y*ku80*Δ*rad9*Δ cells show higher signal compared to wild type, linked to hyper-
922 resection.
923 (B) ChIP-qPCR with a Rad52 antibody around the induced DSB at *MAT* locus in G1 synchronized
924 cells. *rad9Δyku80Δ* and *rad9Δyku80Δesa1-ts* cells show higher signal for Rad52 than wild type
925 but no significant difference by the addition of the *esa1 ts* allele.
926 (C) HO cutting efficiency in wild type, *rad9Δyku80Δ* and *rad9Δyku80Δesa1-ts* cells at the *MAT*
927 locus in G1 synchronized cells after 3 hours of galactose induction.
928
929 **S6 Fig. Nej1 acetylation mutants do not disrupt DNA damage induced phosphorylation but**
930 **affect binding to Mre11.**
931 (A) Nej1 is acetylated *in vivo* on residues K18, K192 and K234 in a NuA4-dependent manner. Mass
932 spectrometry analysis of Nej1 lysine acetylation sites in *ESA1* wild type and temperature sensitive
933 (ts) mutant. See full peptide sequences in Table S2.
934 (B) Nej1 wild-type and lysine mutants show similar ability to repair a chromosomal DSB induced
935 at *MAT* locus by HO induction in the absence of *HML/HMR* donor sequence.

936 (C) HO cutting efficiency at *MAT* locus in G1 synchronized cells after 3 hours of galactose
937 induction in the indicated *nej1*Δ strains.
938 (D) *In vitro* protein pull-down assay showing that recombinant wild type Nej1 and Nej1-3KR bind
939 to the C-terminal region of rMre11, while this interaction is much reduced with Nej1-3KQ. Empty
940 GST was used as negative control.
941 (E) Nej1 lysine mutants do not affect the DNA damage induced phosphorylation of Nej1. Western
942 blot analysis of whole cell extracts (WCE) prepared from indicated yeast strains treated with MMS
943 (0.05%) or DMSO (control) for 2 hours. Pgk1 was used as loading control.
944 (F) Western blot analysis on WCE showing depletion of Esa1 does not affect the DNA damage
945 induced phosphorylation of Nej1. Esa1 was FRB tagged and depleted from the nucleus using the
946 anchor-away system in presence of rapamycin [24]. This was followed by treatment of cells with
947 MMS or DMSO. Pgk1 was used as loading control.
948 (G) Western blot analysis of yeast WCE showing reduced acetylation of H4 in the anchor-away
949 background with Esa1 FRB tagged after rapamycin treatment. H2B was used as loading control.
950
951 **S1 Table: Yeast strains used in the current study**
952
953 **S2 Table: Acetylated peptides detected by mass spectrometry in *ESA1* and *esa1* ts strains**
954 List of Nej1 peptides containing an acetylated lysine residue confidently identified by mass
955 spectrometry after affinity purification from extracts of WT and *esa1 ts* cells and trypsin
956 digestion. Total peptide sequence coverage obtained were 77 and 83% respectively.
957

1 **S1 Table: Yeast strains used in the current study**

Strain	**Genotype**	**Reference**
JKM139	*MATa hoΔ hmlΔ::ADE1 hmrΔ::ADE1 ade1-100 leu2-3;112 lys5 trp1::hisG ura3-52 ade3::GAL-HO*	[75]
QY2211	JKM139 *bar1Δ::NATMX*	This study
QY2212	JKM139 *bar1Δ::NATMX rad9Δ::KANMX*	This study
QY2213	JKM139 *bar1Δ::NATMX yku80Δ*::*TRP1*	This study
QY2214	JKM139 *bar1Δ::NATMX rad9Δ::KANMX yku80Δ*::*TRP1*	This study
QY2231	JKM139 *bar1Δ::LEU2 rad9Δ::KANMX yku80Δ*::*TRP1 esa1-L254P::NATMX*	This study
QY2215	JKM139 *bar1Δ::NATMX nej1Δ*::*TRP1*	This study
QY2216	JKM139 *bar1Δ::NATMX xrs2Δ*::*TRP1*	This study
QY2217	JKM139 *bar1Δ::NATMX rad9Δ::KANMX xrs2Δ*::*TRP1*	This study
QY2218	JKM139 *bar1Δ::NATMX rad9Δ::KANMX xrs2Δ*::*TRP1 yku80Δ*::*HPHMX*	This study
QY2219	JKM139 *bar1Δ::NATMX mre11-H125N::HPHMX*	This study
QY2220	JKM139 *bar1Δ::NATMX* + (pRS416)	This study
QY2221	JKM139 *bar1Δ::NATMX xrs2Δ*::*TRP1* + (pRS416)	This study
QY2222	JKM139 *bar1Δ::NATMX xrs2Δ*::*TRP1* + (pRS416 *MRE11-NLS*)	This study
QY2223	JKM139 *bar1Δ::NATMX rad9Δ::KANMX xrs2Δ*::*TRP1 yku80Δ*::*HPHMX* + (pRS416 *MRE11-NLS*)	This study
QY2260	JKM139 *bar1Δ::NATMX xrs2Δ*::*TRP1* + (pRS416 *MRE11-NLS-X85*)	This study

QY2261	JKM139 *bar1Δ::NATMX rad9Δ::KANMX xrs2Δ*::*TRP1 yku80Δ*::*HPHMX* + (pRS416 *MRE11-NLS-X85*)	This study
QY1603	JKM139 *sml1::NATMX*	[23]
QY2224	QY1603 + (pRS416)	This study
QY2259	QY1603 *xrs2Δ::LEU2* + (pRS416) + (pRS424 *TRP1 2μ ori*)	This study
QY2258	QY1603 *xrs2Δ::LEU2* + (pRS416 *MRE11-NLS*) + (pRS424 *TRP1 2μ ori*)	This study
QY2256	QY1603 *xrs2Δ::LEU2* + (pRS416 *MRE11-NLS*) + (pRS424 *EXO1 TRP1 2μ ori*)	This study
QY2257	QY1603 *xrs2Δ::LEU2* + (pRS416 *MRE11-NLS*) + (pRS424 *EXO1-D173A TRP1 2μ ori*)	This study
QY1604	JKM139 *sml1::NATMX lcd1::KANMX*	[23]
QY2225	QY1604 + (pRS416)	This study
QY-2226	QY1604 *xrs2Δ::LEU2* + (pRS416)	This study
QY2227	QY1604 *xrs2Δ::LEU2* + (pRS416 *MRE11-NLS*)	This study
QY2228	QY2227 + (pRS424 *TRP1 2μ ori*)	This study
QY2229	QY2227 + (pRS424 *EXO1 TRP1 2μ ori*)	This study
QY2230	QY2227 + (pRS424 *EXO1-D173A TRP1 2μ ori*)	This study
QY2600	BY4741 *MATa his3Δ1 leu2Δ0 met15Δ0 ura3Δ0 nej1Δ*::*KANMX*	This study
QY2232	QY2600 + (pRS413)	This study
QY2233	QY2600 + (pRS413 *NEJ1*)	This study
QY2234	QY2600 + (pRS413 *NEJ1-K18R-K192R-K234R*)	This study
QY2235	QY2600 + (pRS413 *NEJ1-K18Q-K192Q-K234Q*)	This study

QY2236	QY2215 + (pRS416)	This study
QY2237	QY2215 + (pRS416 *NEJ1*)	This study
QY2238	QY2215 + (pRS416 *NEJ1-K18R-K192R-K234R*)	This study
QY2239	QY2215 + (pRS416 *NEJ1-K18Q-K192Q-K234Q)*	This study
QY3572	JKM139 *fpr1Δ::HphMX tor1-1::URA3 RPL13A-2*FKBP12::TRP1 FRB-ESA1::KanMX*	[64]
QY2240	QY3572 *YKU80-13MYC::NATMX*	This study
QY2241	QY3572 *NEJ1-13MYC::NATMX*	This study
QY2054	BY4741 *MATa his3Δ1 leu2Δ0 met15Δ0 ura3Δ0* +pEGH(GAL-GST-Nej1)	Open Biosystem
QY2058	BY4741 *MATa his3Δ1 leu2Δ0 met15Δ0 ura3Δ0 esa1Δ::KanMX* +pSAPE5(HA-*esa1-L254P LEU2 ARS/CEN*) +pEGH(GAL-GST-Nej1)	This study
tNS2333	*ho*Δ *hml*Δ::*ADE1 mat***a**Δ::*hisG hmr*Δ::*ADE1 his4*::[*NAT-leu2*(Asp718-SalI)] *leu2*::*HOcs ade3*::*GAL*::*HO ade1 lys5 ura3-52 TyΔ*	[49]
QY2266	tNS2333 *rad51Δ::KAN*	This study
QY2264	tNS2333 *esa1-L254P::NATMX*	This study
QY2267	tNS2333 *esa1-L254P::NATMX rad51Δ::KAN*	This study
QY2265	tNS2333 *rad52Δ::NAT*	This study

2

3 **S2 Table: Acetylated peptides detected by mass spectrometry in *ESA1* and *esa1* ts strains**

Yeast strain	Sequence position	Peptide sequence
ESA1-WT	aa 7-19	GQQLSDAEWCVKacK
	aa 163-174	QKacCLDFLLISLR
	aa 182-208	VISQWAPENSKacNYESLQQCTDDDIIKK
	aa 193-208	NYESLQQCTDDDIIKacK
	aa 213-226	GKacFQHQEFLADSLK
	aa 233-240	NKacFQDVSR
	aa 305-319	LENFSESEATPEKacTK
esa1-L254P	aa 163-174	QKacCLDFLLISLR
	aa 193-208	NYESLQQCTDDDIIKacK
	aa 213-226	GKacFQHQEFLADSLK
	aa 305-319	LENFSESEATPEKacTK

4
5

6

FIGURE 1

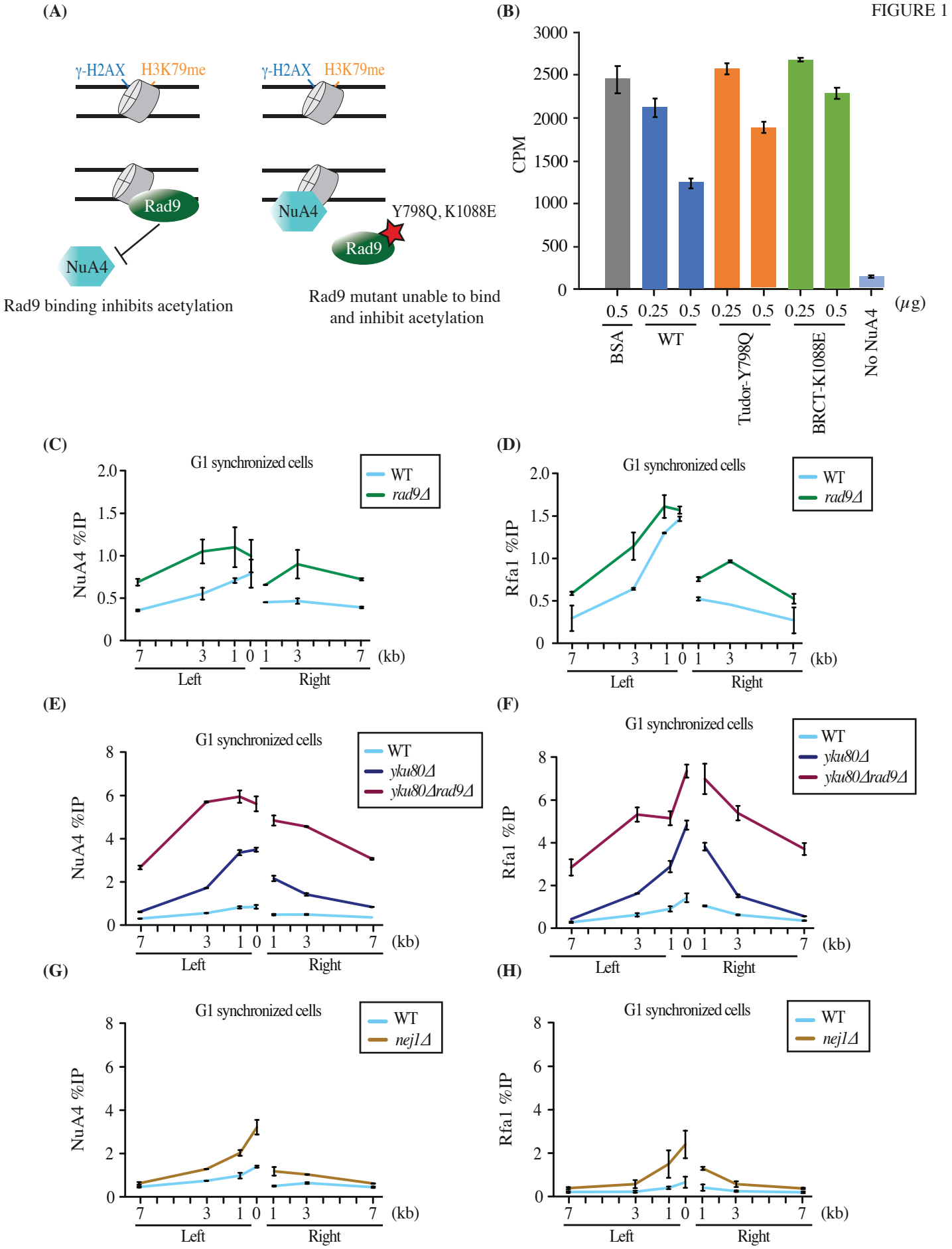
(A)
γ-H2AX
H3K79me
Rad9
NuA4
Rad9 binding inhibits acetylation
γ-H2AX
H3K79me
NuA4
Y798Q, K1088E
Rad9
Rad9 mutant unable to bind and inhibit acetylation
(B)
CPM
3000
2500
2000
1500
1000
500
0
0.5 0.25 0.5 0.25 0.5 0.25 0.5
(μg)
BSA
WT
Tudor-Y798Q
BRCT-K1088E
No NuA4
(C)
G1 synchronized cells
WT
rad9Δ
NuA4 %IP
2.0
1.5
1.0
0.5
0
7 3 1 0 1 3 7 (kb)
Left
Right
(D)
G1 synchronized cells
WT
rad9Δ
Rfa1 %IP
2.0
1.5
1.0
0.5
0
7 3 1 0 1 3 7 (kb)
Left
Right
(E)
G1 synchronized cells
WT
yku80Δ
yku80Δrad9Δ
NuA4 %IP
8
6
4
2
0
7 3 1 0 1 3 7 (kb)
Left
Right
(F)
G1 synchronized cells
WT
yku80Δ
yku80Δrad9Δ
Rfa1 %IP
8
6
4
2
0
7 3 1 0 1 3 7 (kb)
Left
Right
(G)
G1 synchronized cells
WT
nej1Δ
NuA4 %IP
8
6
4
2
0
7 3 1 0 1 3 7 (kb)
Left
Right
(H)
G1 synchronized cells
WT
nej1Δ
Rfa1 %IP
8
6
4
2
0
7 3 1 0 1 3 7 (kb)
Left
Right

FIGURE 2

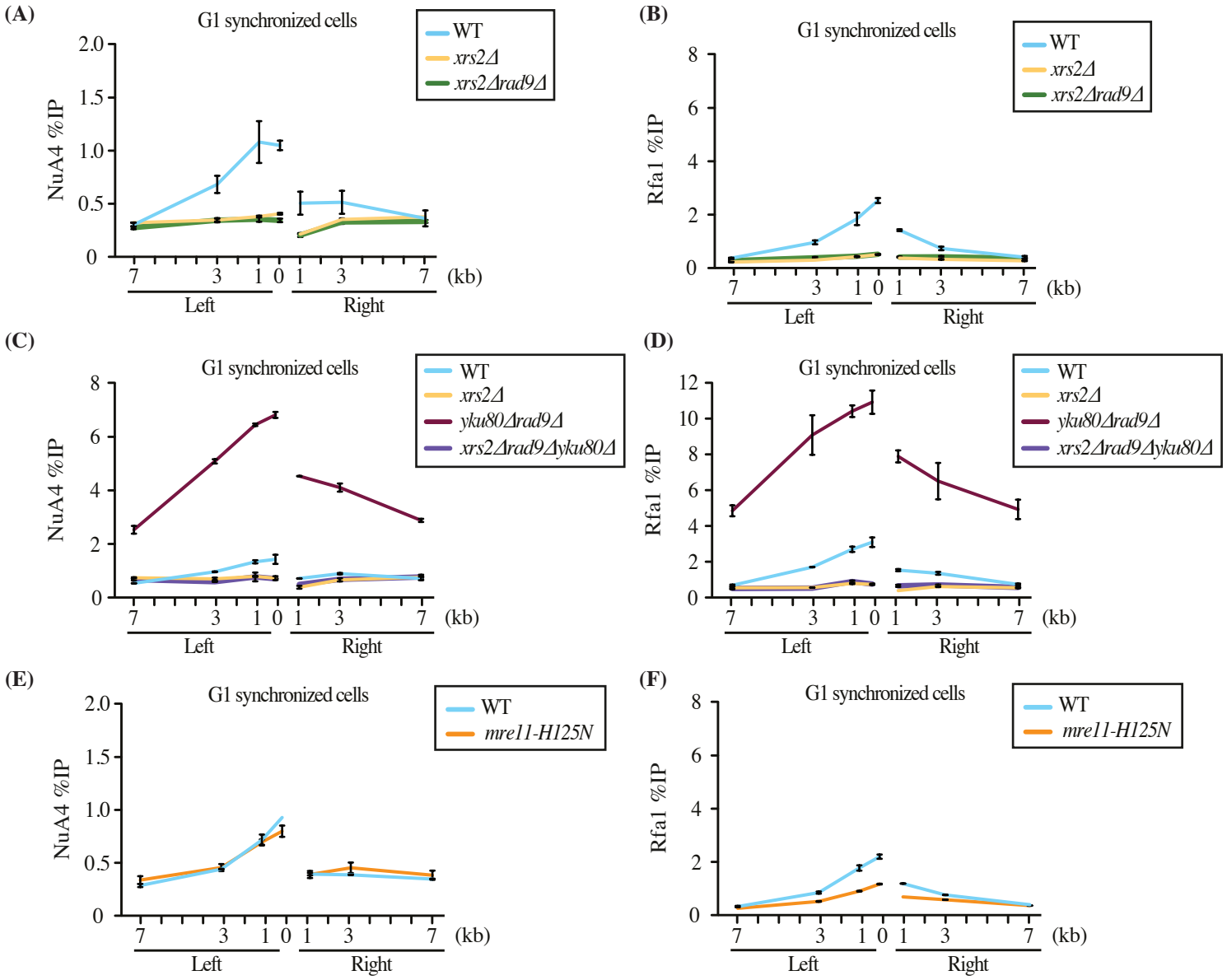
(A)
G1 synchronized cells
WT
xrs2Δ
xrs2Δrad9Δ
NuA4 %IP
2.0
1.5
1.0
0.5
0
7
3
1
0
1
3
7
(kb)
Left
Right
(B)
G1 synchronized cells
WT
xrs2Δ
xrs2Δrad9Δ
Rfa1 %IP
8
6
4
2
0
7
3
1
0
1
3
7
(kb)
Left
Right
(C)
G1 synchronized cells
WT
xrs2Δ
yku80Δrad9Δ
xrs2Δrad9Δyku80Δ
NuA4 %IP
8
6
4
2
0
7
3
1
0
1
3
7
(kb)
Left
Right
(D)
G1 synchronized cells
WT
xrs2Δ
yku80Δrad9Δ
xrs2Δrad9Δyku80Δ
Rfa1 %IP
12
10
8
6
4
2
0
7
3
1
0
1
3
7
(kb)
Left
Right
(E)
G1 synchronized cells
WT
mre11-H125N
NuA4 %IP
2.0
1.5
1.0
0.5
0
7
3
1
0
1
3
7
(kb)
Left
Right
(F)
G1 synchronized cells
WT
mre11-H125N
Rfa1 %IP
8
6
4
2
0
7
3
1
0
1
3
7
(kb)
Left
Right

FIGURE 3

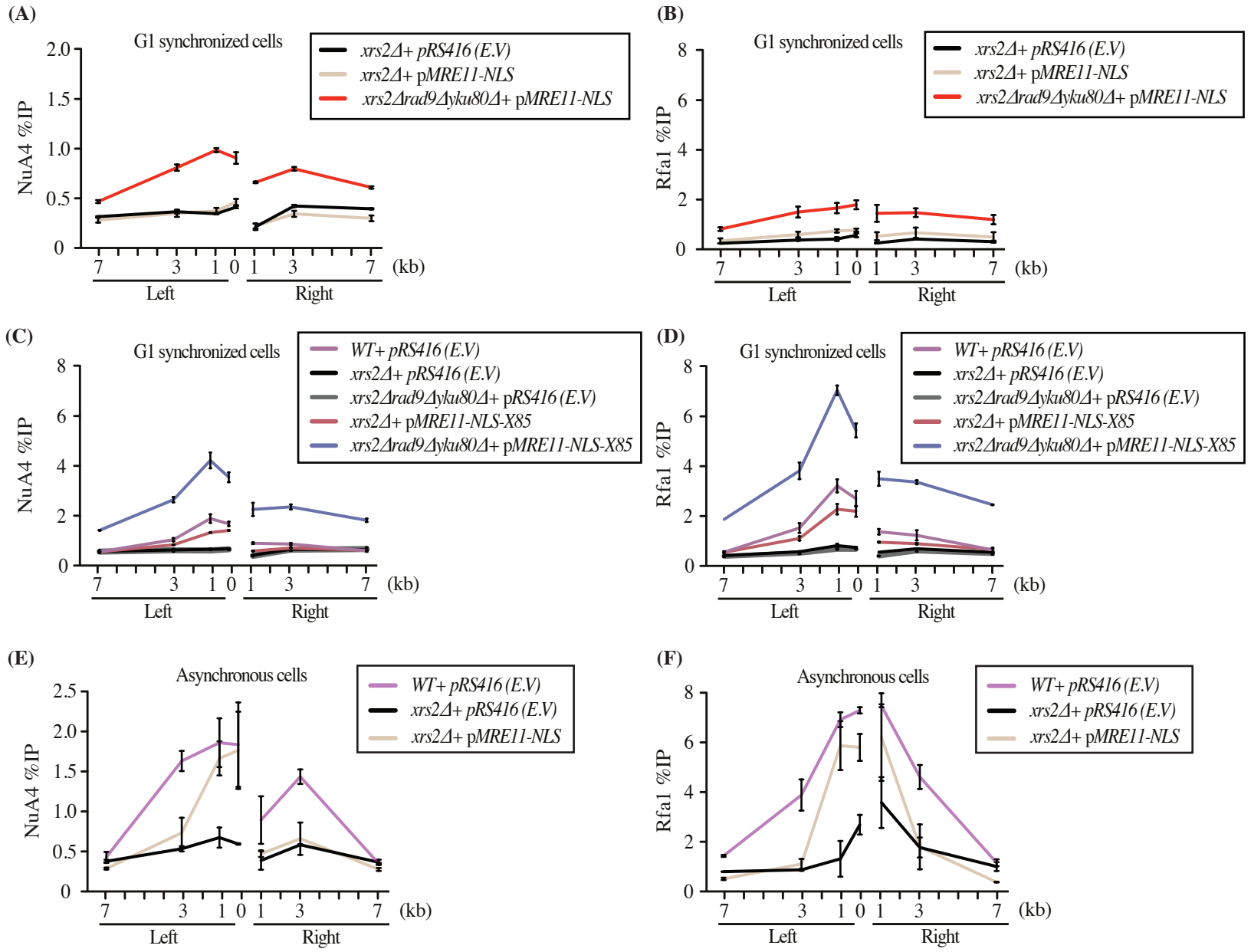
(A)
G1 synchronized cells
xrs2Δ+ pRS416 (E.V)
xrs2Δ+ pMRE11-NLS
xrs2Δrad9Δyku80Δ+ pMRE11-NLS
NuA4 %IP
Left
Right
(kb)
(B)
G1 synchronized cells
xrs2Δ+ pRS416 (E.V)
xrs2Δ+ pMRE11-NLS
xrs2Δrad9Δyku80Δ+ pMRE11-NLS
Rfa1 %IP
Left
Right
(kb)
(C)
G1 synchronized cells
WT+ pRS416 (E.V)
xrs2Δ+ pRS416 (E.V)
xrs2Δrad9Δyku80Δ+ pRS416 (E.V)
xrs2Δ+ pMRE11-NLS-X85
xrs2Δrad9Δyku80Δ+ pMRE11-NLS-X85
NuA4 %IP
Left
Right
(kb)
(D)
G1 synchronized cells
WT+ pRS416 (E.V)
xrs2Δ+ pRS416 (E.V)
xrs2Δrad9Δyku80Δ+ pRS416 (E.V)
xrs2Δ+ pMRE11-NLS-X85
xrs2Δrad9Δyku80Δ+ pMRE11-NLS-X85
Rfa1 %IP
Left
Right
(kb)
(E)
Asynchronous cells
WT+ pRS416 (E.V)
xrs2Δ+ pRS416 (E.V)
xrs2Δ+ pMRE11-NLS
NuA4 %IP
Left
Right
(kb)
(F)
Asynchronous cells
WT+ pRS416 (E.V)
xrs2Δ+ pRS416 (E.V)
xrs2Δ+ pMRE11-NLS
Rfa1 %IP
Left
Right
(kb)

FIGURE 4

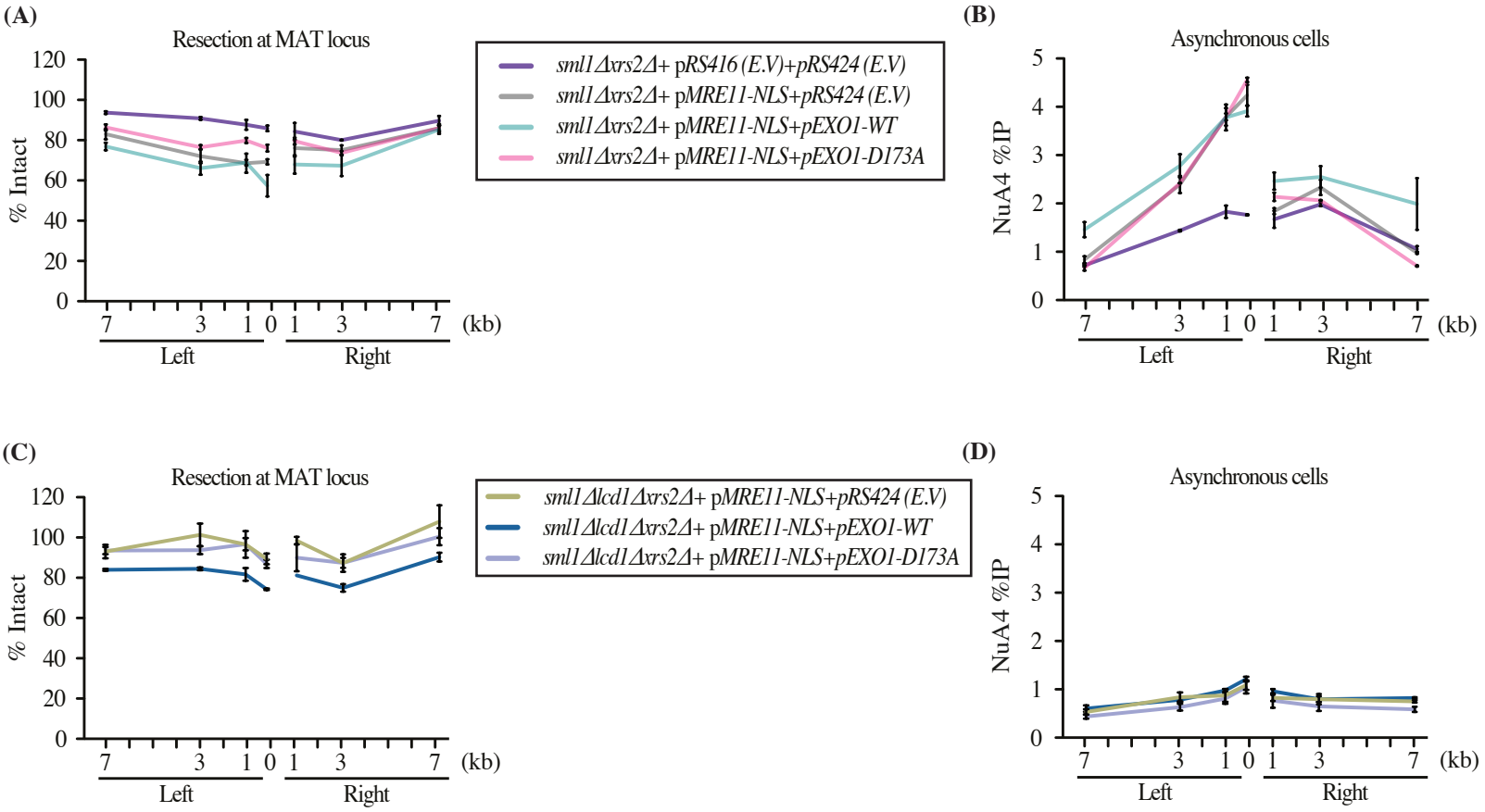
(A)
Resection at MAT locus
% Intact
120
100
80
60
40
20
0
7
3
1
0
1
3
7
(kb)
Left
Right
sml1Δxrs2Δ+ pRS416 (E.V)+pRS424 (E.V)
sml1Δxrs2Δ+ pMRE11-NLS+pRS424 (E.V)
sml1Δxrs2Δ+ pMRE11-NLS+pEXO1-WT
sml1Δxrs2Δ+ pMRE11-NLS+pEXO1-D173A
(B)
Asynchronous cells
NuA4 %IP
5
4
3
2
1
0
7
3
1
0
1
3
7
(kb)
Left
Right
(C)
Resection at MAT locus
% Intact
120
100
80
60
40
20
0
7
3
1
0
1
3
7
(kb)
Left
Right
sml1Δlcd1Δxrs2Δ+ pMRE11-NLS+pRS424 (E.V)
sml1Δlcd1Δxrs2Δ+ pMRE11-NLS+pEXO1-WT
sml1Δlcd1Δxrs2Δ+ pMRE11-NLS+pEXO1-D173A
(D)
Asynchronous cells
NuA4 %IP
5
4
3
2
1
0
7
3
1
0
1
3
7
(kb)
Left
Right

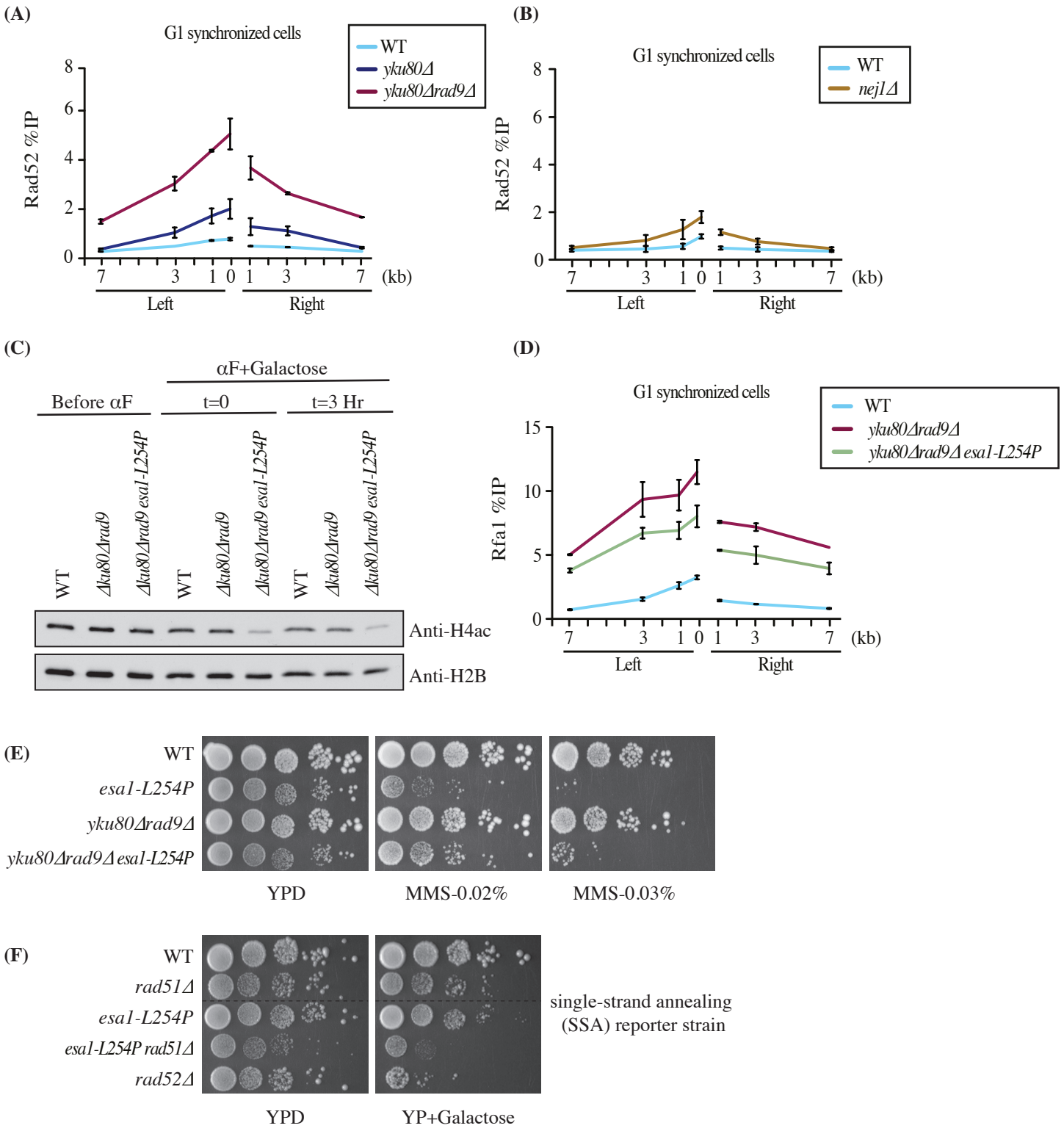
(A)
G1 synchronized cells
WT
yku80Δ
yku80Δrad9Δ
Rad52 %IP
8
6
4
2
0
7
3
1
0
1
3
7
(kb)
Left
Right
(B)
G1 synchronized cells
WT
nej1Δ
Rad52 %IP
8
6
4
2
0
7
3
1
0
1
3
7
(kb)
Left
Right
(C)
αF+Galactose
Before αF
t=0
t=3 Hr
WT
Δku80Δrad9
Δku80Δrad9 esa1-L254P
WT
Δku80Δrad9
Δku80Δrad9 esa1-L254P
WT
Δku80Δrad9
Δku80Δrad9 esa1-L254P
Anti-H4ac
Anti-H2B
(D)
G1 synchronized cells
WT
yku80Δrad9Δ
yku80Δrad9Δ esa1-L254P
Rfa1 %IP
15
10
5
0
7
3
1
0
1
3
7
(kb)
Left
Right
(E)
WT
esa1-L254P
yku80Δrad9Δ
yku80Δrad9Δ esa1-L254P
YPD
MMS-0.02%
MMS-0.03%
(F)
WT
rad51Δ
esa1-L254P
esa1-L254P rad51Δ
rad52Δ
YPD
YP+Galactose
single-strand annealing
(SSA) reporter strain

FIGURE 6

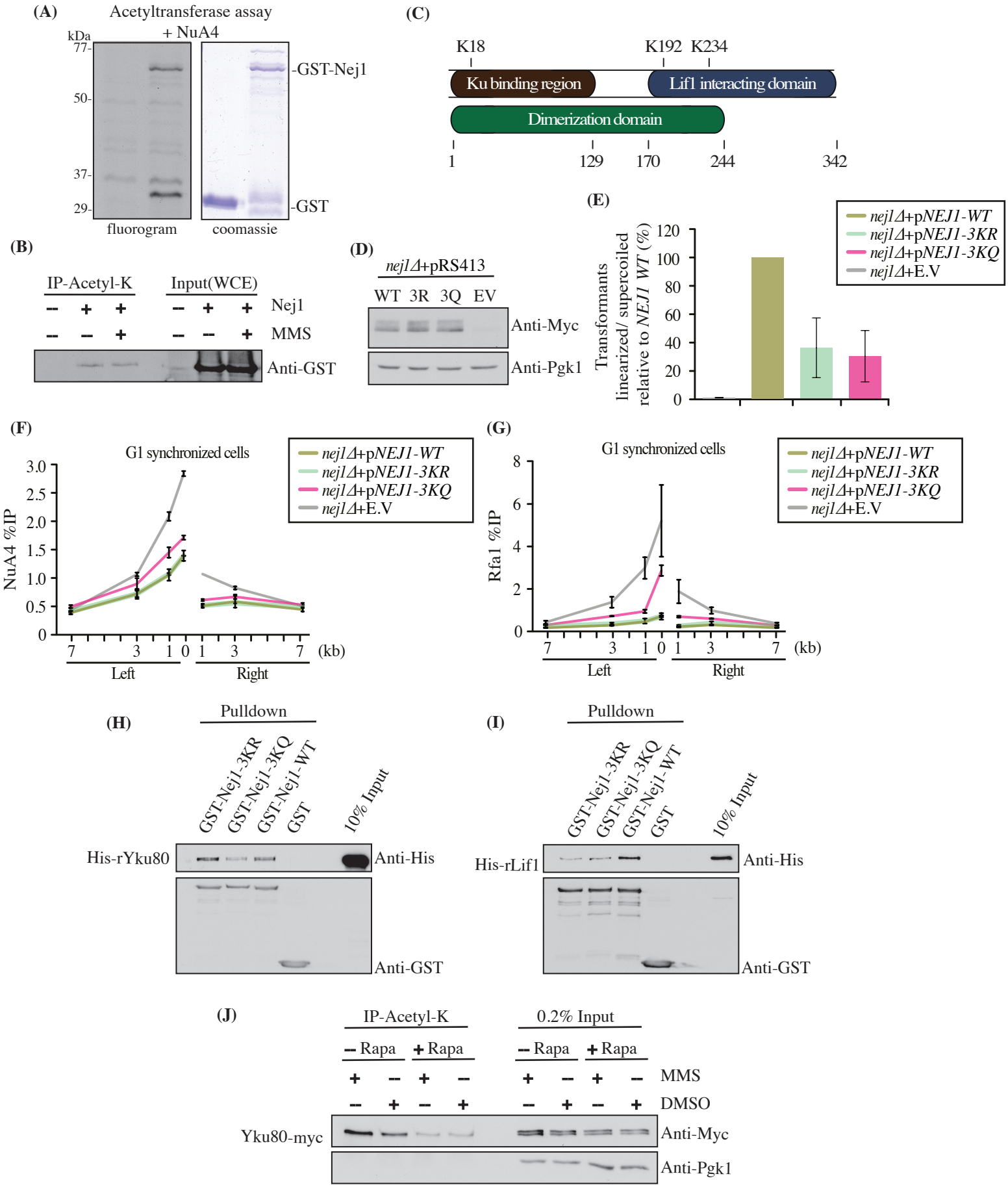
(A)
Acetyltransferase assay
+ NuA4
kDa
77-
50-
37-
29-
-GST-Nej1
-GST
fluorogram
coomassie
(B)
IP-Acetyl-K
Input(WCE)
Nej1
MMS
Anti-GST
(C)
K18
K192
K234
Ku binding region
Lif1 interacting domain
Dimerization domain
1
129
170
244
342
(D)
nej1Δ+pRS413
WT
3R
3Q
EV
Anti-Myc
Anti-Pgk1
(E)
Transformants linearized/ supercoiled relative to NEJ1 WT (%)
nej1Δ+pNEJ1-WT
nej1Δ+pNEJ1-3KR
nej1Δ+pNEJ1-3KQ
nej1Δ+E.V
(F)
G1 synchronized cells
NuA4 %IP
Left
Right
(kb)
(G)
G1 synchronized cells
Rfa1 %IP
Left
Right
(kb)
(H)
Pulldown
GST-Nej1-3KR
GST-Nej1-3KQ
GST-Nej1-WT
GST
10% Input
His-rYku80
Anti-His
Anti-GST
(I)
Pulldown
GST-Nej1-3KR
GST-Nej1-3KQ
GST-Nej1-WT
GST
10% Input
His-rLif1
Anti-His
Anti-GST
(J)
IP-Acetyl-K
0.2% Input
– Rapa
+ Rapa
MMS
DMSO
Yku80-myc
Anti-Myc
Anti-Pgk1

FIGURE 7

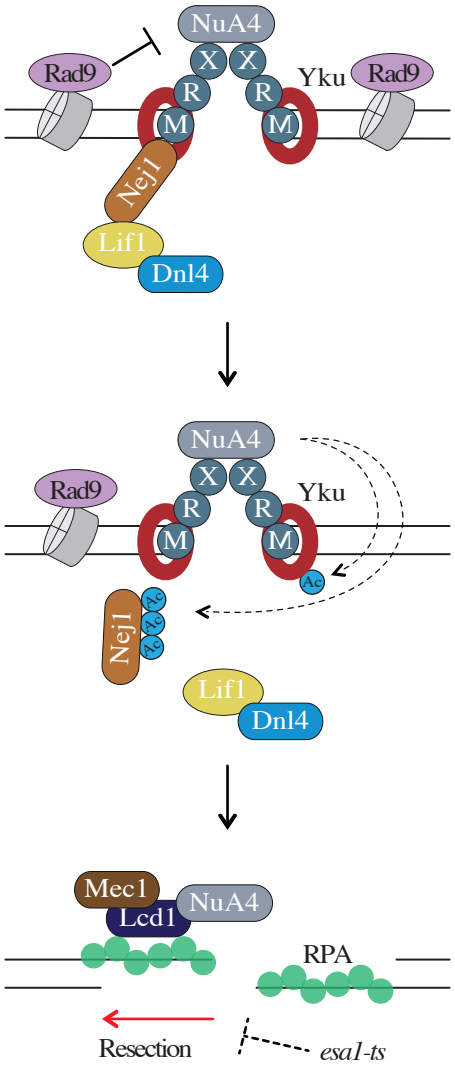
NuA4
X
X
R
R
M
M
Rad9
Yku
Rad9
Nej1
Lif1
Dnl4
NuA4
X
X
R
R
M
M
Rad9
Yku
Ac
Nej1
Ac
Ac
Ac
Lif1
Dnl4
Mec1
Lcd1
NuA4
RPA
Resection
esa1-ts

S1 Fig

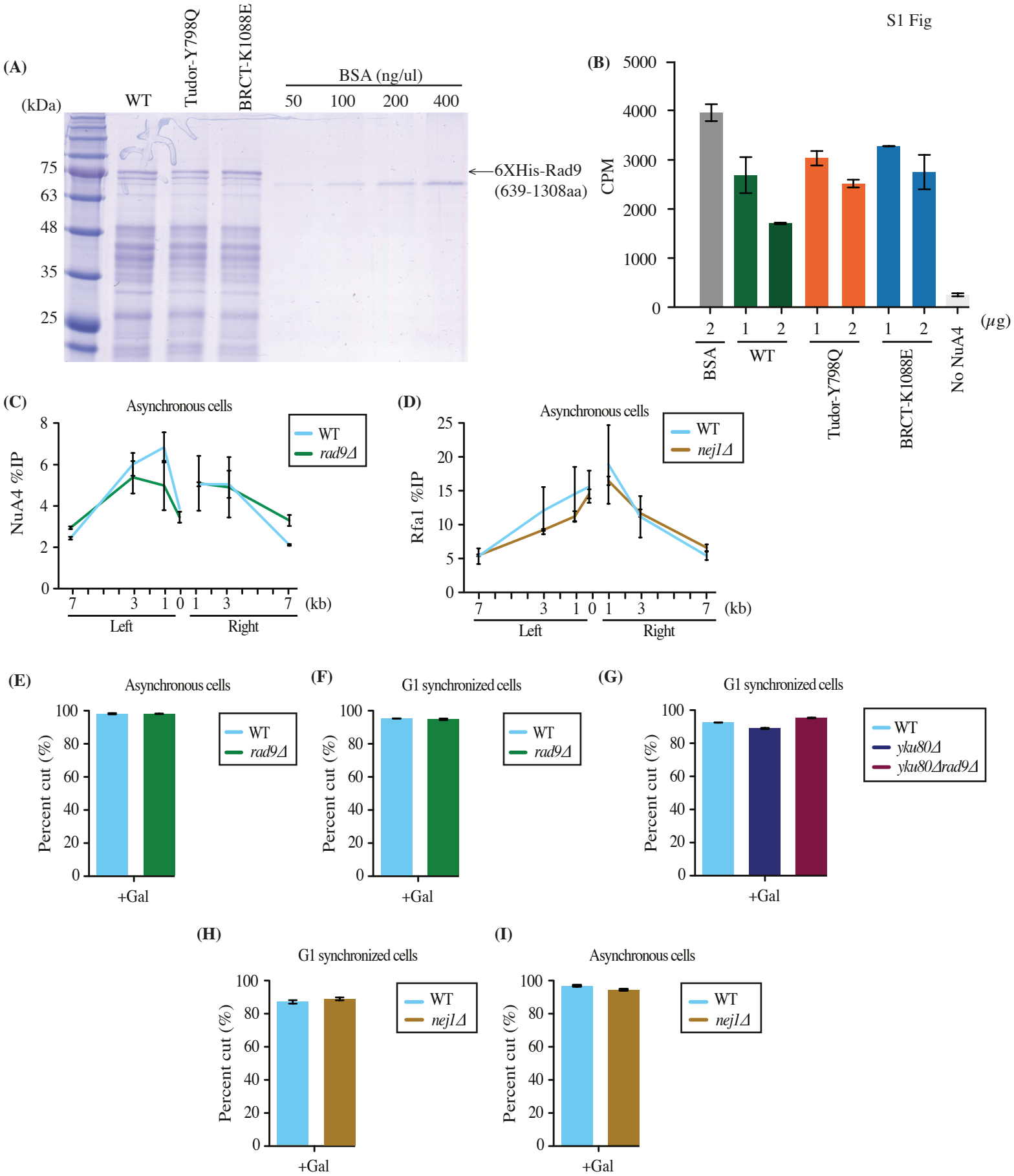
(A)
(kDa)
WT
Tudor-Y798Q
BRCT-K1088E
BSA (ng/ul)
50
100
200
400
75
63
48
35
25
6XHis-Rad9
(639-1308aa)
(B)
CPM
5000
4000
3000
2000
1000
0
2
1
2
1
2
1
2
(μg)
BSA
WT
Tudor-Y798Q
BRCT-K1088E
No NuA4
(C)
Asynchronous cells
NuA4 %IP
WT
rad9Δ
7
3
1
0
1
3
7
(kb)
Left
Right
(D)
Asynchronous cells
Rfa1 %IP
WT
nej1Δ
(E)
Asynchronous cells
Percent cut (%)
+Gal
(F)
G1 synchronized cells
(G)
G1 synchronized cells
yku80Δ
yku80Δrad9Δ
(H)
G1 synchronized cells
(I)
Asynchronous cells

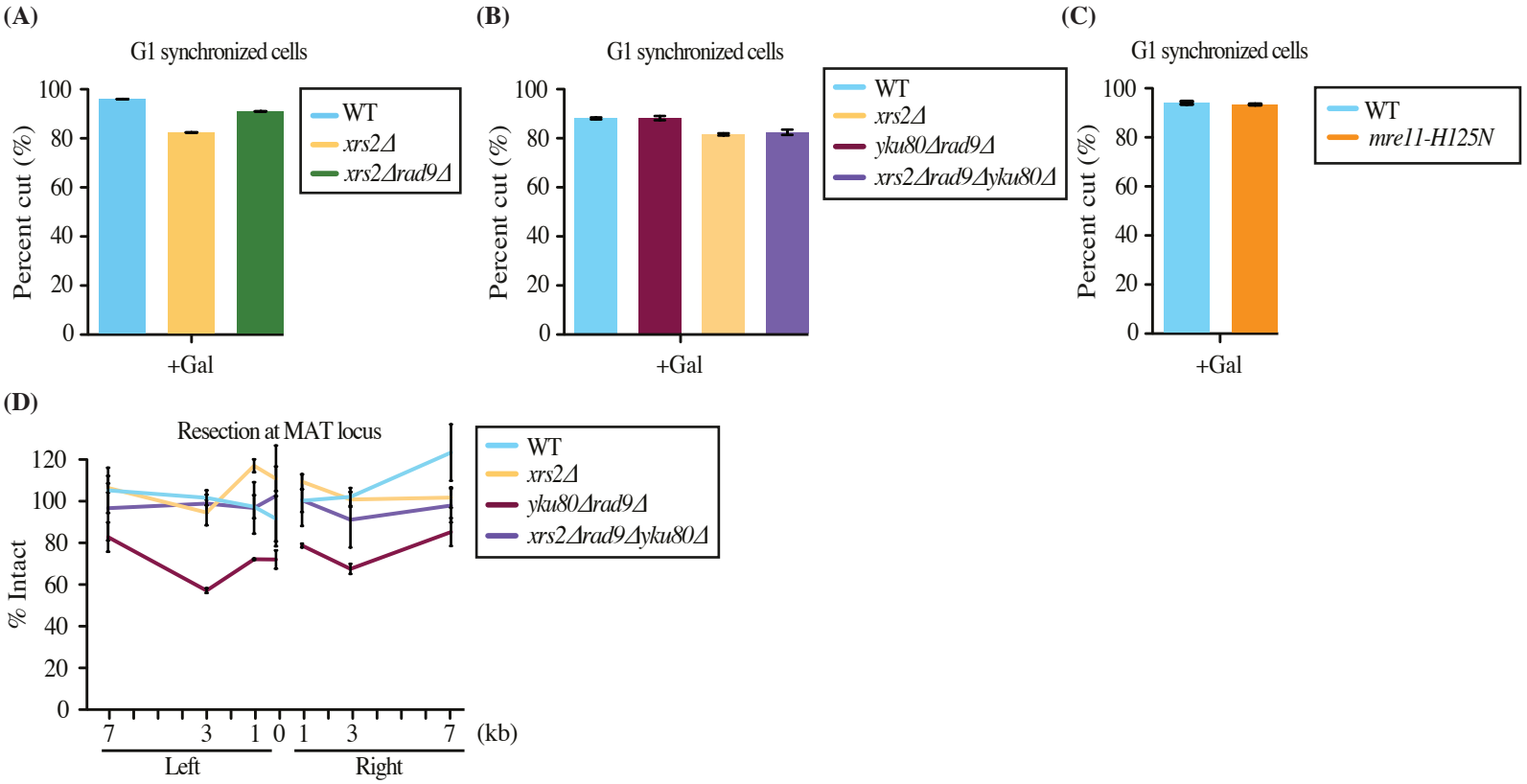
(A)
G1 synchronized cells
Percent cut (%)
100
80
60
40
20
0
+Gal
WT
xrs2Δ
xrs2Δrad9Δ
(B)
G1 synchronized cells
Percent cut (%)
+Gal
WT
xrs2Δ
yku80Δrad9Δ
xrs2Δrad9Δyku80Δ
(C)
G1 synchronized cells
Percent cut (%)
+Gal
WT
mre11-H125N
(D)
Resection at MAT locus
% Intact
120
100
80
60
40
20
0
7
3
1
0
1
3
7
(kb)
Left
Right
WT
xrs2Δ
yku80Δrad9Δ
xrs2Δrad9Δyku80Δ

S3 Fig

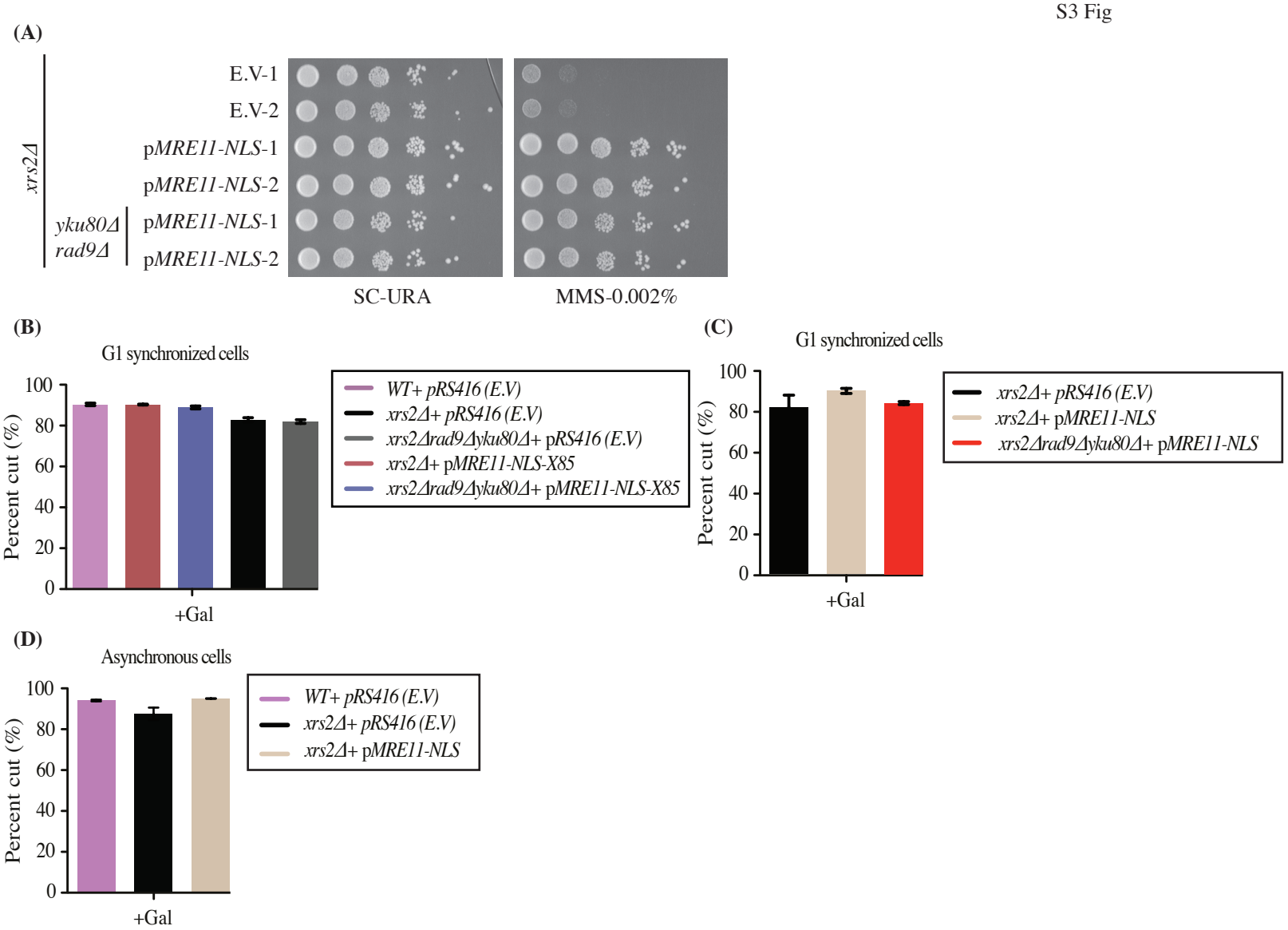
(A)
xrs2Δ
E.V-1
E.V-2
pMRE11-NLS-1
pMRE11-NLS-2
yku80Δ
rad9Δ
pMRE11-NLS-1
pMRE11-NLS-2
SC-URA
MMS-0.002%
(B)
G1 synchronized cells
Percent cut (%)
100
80
60
40
20
0
+Gal
WT+ pRS416 (E.V)
xrs2Δ+ pRS416 (E.V)
xrs2Δrad9Δyku80Δ+ pRS416 (E.V)
xrs2Δ+ pMRE11-NLS-X85
xrs2Δrad9Δyku80Δ+ pMRE11-NLS-X85
(C)
G1 synchronized cells
Percent cut (%)
100
80
60
40
20
0
+Gal
xrs2Δ+ pRS416 (E.V)
xrs2Δ+ pMRE11-NLS
xrs2Δrad9Δyku80Δ+ pMRE11-NLS
(D)
Asynchronous cells
Percent cut (%)
100
80
60
40
20
0
+Gal
WT+ pRS416 (E.V)
xrs2Δ+ pRS416 (E.V)
xrs2Δ+ pMRE11-NLS

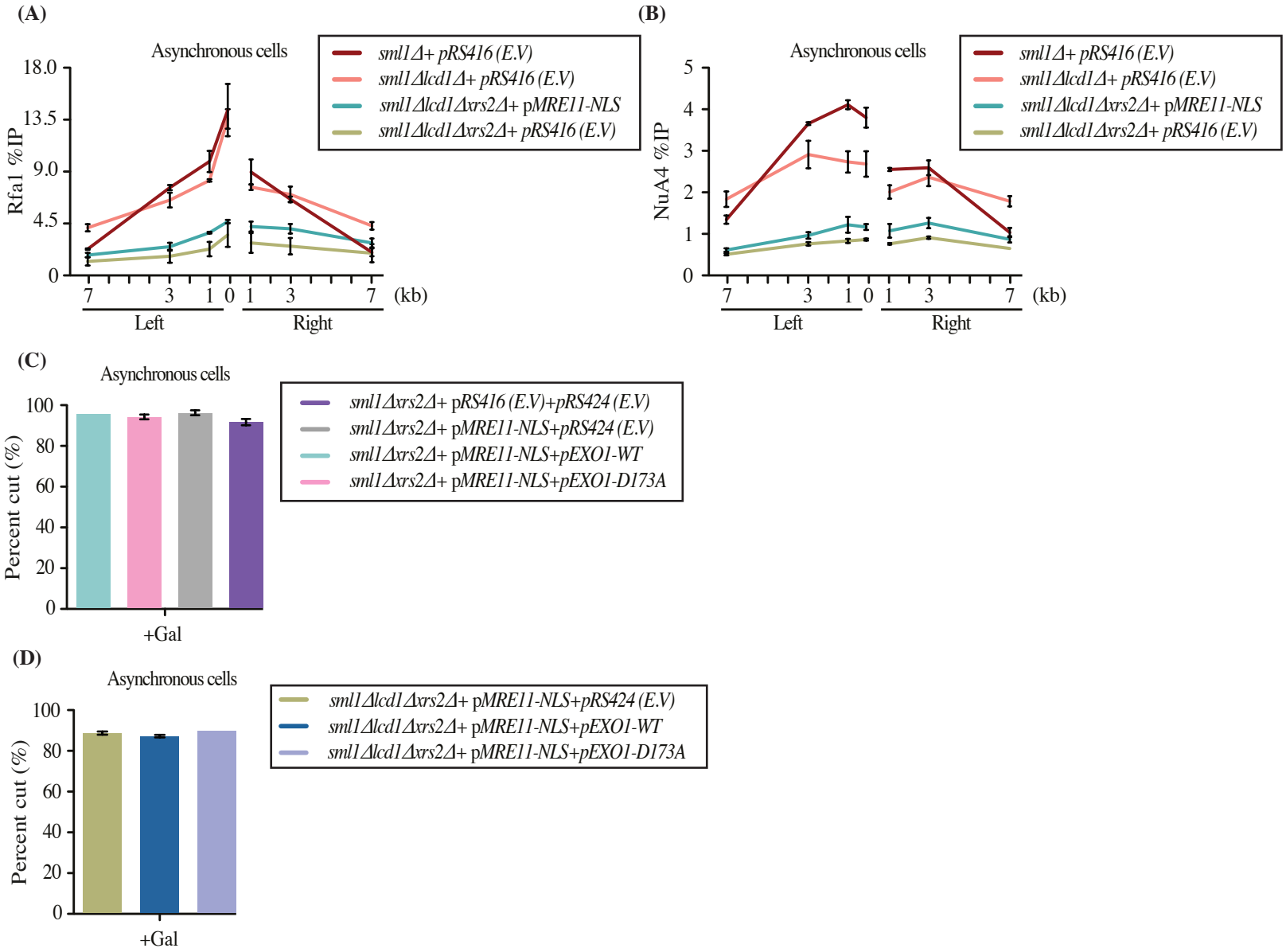
(A)
Asynchronous cells
Rfa1 %IP
18.0
13.5
9.0
4.5
0
7
3
1
0
1
3
7
(kb)
Left
Right
sml1Δ+ pRS416 (E.V)
sml1Δlcd1Δ+ pRS416 (E.V)
sml1Δlcd1Δxrs2Δ+ pMRE11-NLS
sml1Δlcd1Δxrs2Δ+ pRS416 (E.V)
(B)
Asynchronous cells
NuA4 %IP
5
4
3
2
1
0
7
3
1
0
1
3
7
(kb)
Left
Right
sml1Δ+ pRS416 (E.V)
sml1Δlcd1Δ+ pRS416 (E.V)
sml1Δlcd1Δxrs2Δ+ pMRE11-NLS
sml1Δlcd1Δxrs2Δ+ pRS416 (E.V)
(C)
Asynchronous cells
Percent cut (%)
100
80
60
40
20
0
+Gal
sml1Δxrs2Δ+ pRS416 (E.V)+pRS424 (E.V)
sml1Δxrs2Δ+ pMRE11-NLS+pRS424 (E.V)
sml1Δxrs2Δ+ pMRE11-NLS+pEXO1-WT
sml1Δxrs2Δ+ pMRE11-NLS+pEXO1-D173A
(D)
Asynchronous cells
Percent cut (%)
100
80
60
40
20
0
+Gal
sml1Δlcd1Δxrs2Δ+ pMRE11-NLS+pRS424 (E.V)
sml1Δlcd1Δxrs2Δ+ pMRE11-NLS+pEXO1-WT
sml1Δlcd1Δxrs2Δ+ pMRE11-NLS+pEXO1-D173A

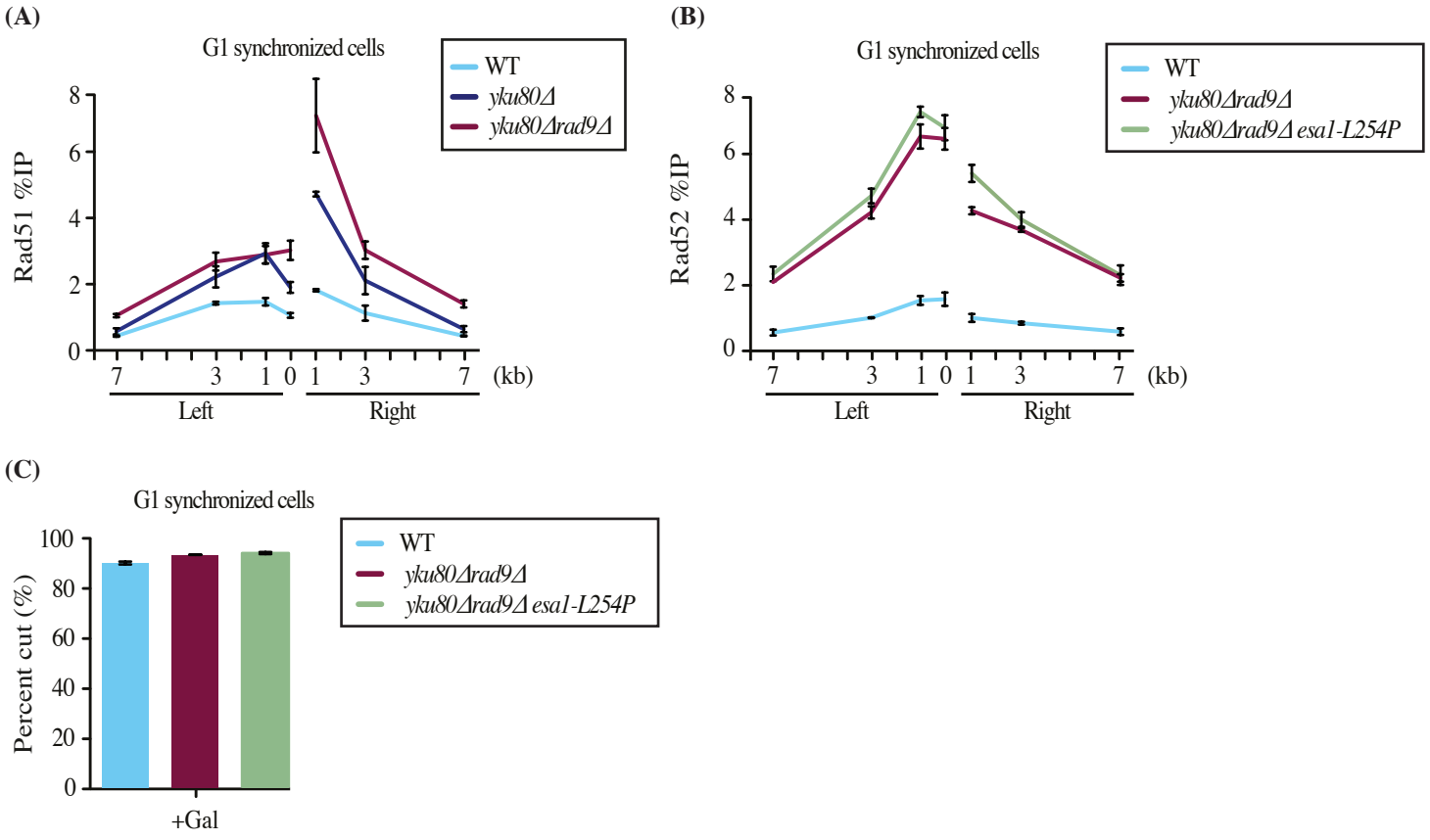
(A)
G1 synchronized cells
Rad51 %IP
WT
yku80Δ
yku80Δrad9Δ
Left
Right
(kb)
(B)
G1 synchronized cells
Rad52 %IP
WT
yku80Δrad9Δ
yku80Δrad9Δ esa1-L254P
Left
Right
(kb)
(C)
G1 synchronized cells
Percent cut (%)
WT
yku80Δrad9Δ
yku80Δrad9Δ esa1-L254P
+Gal

(A)

Ac-Nej1	
Esa1 -WT	*esa1 -ts*
K18	
K164	K164
K192	
K207	K207
K214	K214
K234	
K317	K317

(B)

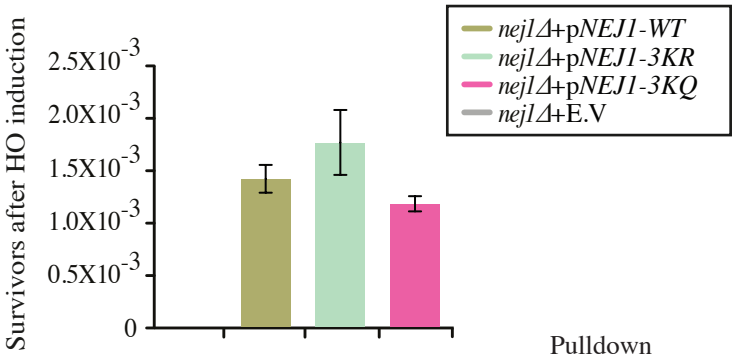

(C)

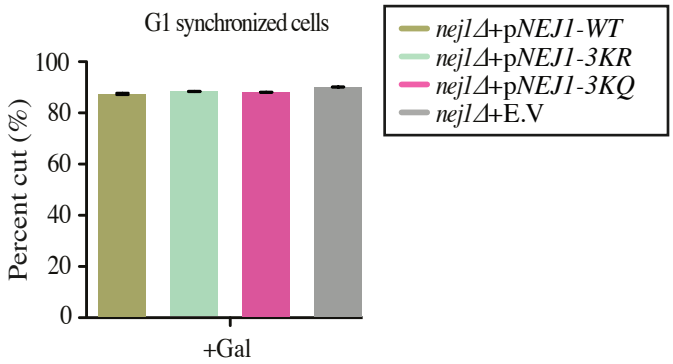

(D)

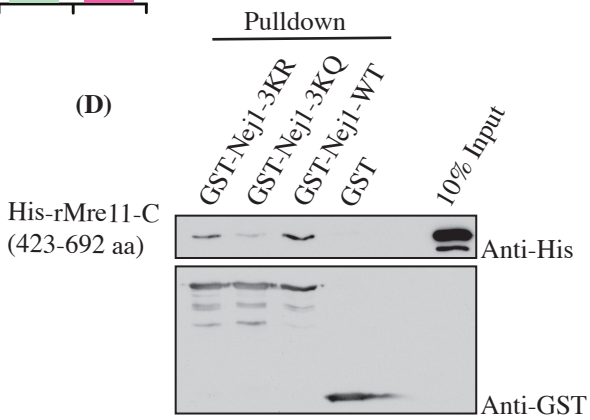

(E)

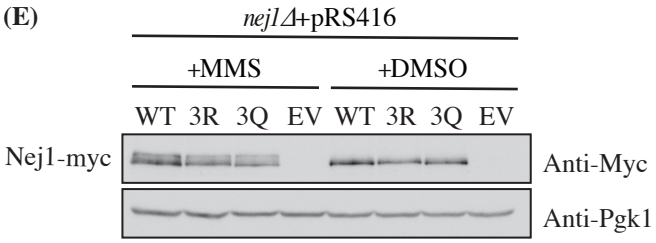

(F)

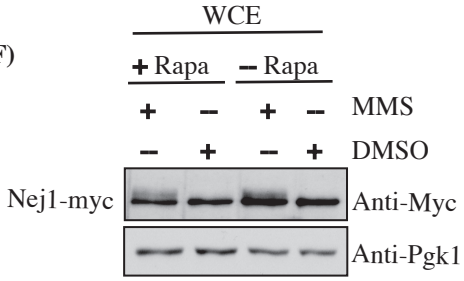
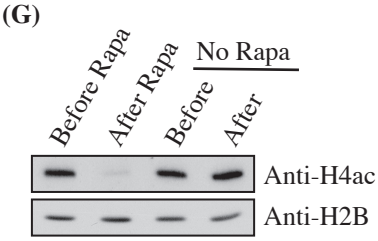
(G)